The *Drosophila melanogaster* Rab GAP RN-tre cross-talks with the Rho1 signaling pathway to regulate nonmuscle myosin II localization and function

Amy Platenkamp[a], Elizabeth Detmar[b], Liz Sepulveda[a], Anna Ritz[a], Stephen L. Rogers[b], and Derek A. Applewhite[a,*]

[a]Department of Biology, Reed College, Portland, OR 97202; [b]Department of Biology & Integrative Program for Biological and Genome Sciences, The University of North Carolina at Chapel Hill, Chapel Hill, NC 27599-3280

ABSTRACT **To identify novel regulators of nonmuscle myosin II (NMII) we performed an image-based RNA interference screen using stable *Drosophila melanogaster* S2 cells expressing the enhanced green fluorescent protein (EGFP)-tagged regulatory light chain (RLC) of NMII and mCherry-Actin. We identified the Rab-specific GTPase-activating protein (GAP) RN-tre as necessary for the assembly of NMII RLC into contractile actin networks. Depletion of RN-tre led to a punctate NMII phenotype, similar to what is observed following depletion of proteins in the Rho1 pathway. Depletion of RN-tre also led to a decrease in active Rho1 and a decrease in phosphomyosin-positive cells by immunostaining, while expression of constitutively active Rho or Rho-kinase (Rok) rescues the punctate phenotype. Functionally, RN-tre depletion led to an increase in actin retrograde flow rate and cellular contractility in S2 and S2R+ cells, respectively. Regulation of NMII by RN-tre is only partially dependent on its GAP activity as overexpression of constitutively active Rabs inactivated by RN-tre failed to alter NMII RLC localization, while a GAP-dead version of RN-tre partially restored phosphomyosin staining. Collectively, our results suggest that RN-tre plays an important regulatory role in NMII RLC distribution, phosphorylation, and function, likely through Rho1 signaling and putatively serving as a link between the secretion machinery and actomyosin contractility.**

Monitoring Editor
Richard Fehon
University of Chicago

Received: Mar 11, 2020
Revised: Jul 17, 2020
Accepted: Aug 3, 2020

INTRODUCTION

Nonmuscle myosin II (NMII) is a ubiquitously expressed motor protein that, when coupled with the actin cytoskeleton, forms an actomyosin network that is largely responsible for contractility in nonmuscle cells. This contractile system is critical to a number of cellular processes, including the morphogenesis that occurs during development, epithelial polarization, cell migration, and adhesion (Vicente-Manzanares *et al.*, 2009; Aguilar-Cuenca *et al.*, 2014). The NMII holoenzyme is a hexamer composed of two heavy chains (encoded by *zipper* in *Drosophila*), two regulatory light chains (RLC, encoded by *Drosophila spaghetti squash* [*sqh*]), and two essential light chains (ELC). The heavy chain can be further divided into three domains: a head domain that binds to actin and ATP, a neck domain that binds Sqh and the ELCs, and a coiled-coil tail domain that first facilitates the formation of dimers and, upon posttranslational modifications, oligomerization (Côté *et al.*, 1984; Winkelmann *et al.*, 1984; Rayment *et al.*, 1993a,b; Newell-Litwa *et al.*, 2015).

Upon phosphorylation of Sqh at residue Ser-19 and/or Thr-18 by serine/threonine kinases, NMII undergoes a conformational change that allows the hexameric unit to form antiparallel minifilament oligomers, composed of 12–15 myosin molecules per filament in

This article was published online ahead of print in MBoC in Press (http://www.molbiolcell.org/cgi/doi/10.1091/mbc.E20-03-0181) on August 20, 2020.

Conflict of interest statement: The authors state that this investigation has been conducted in the absence of any personal, professional, or financial relationships that could be construed as conflicts of interest.

*Address correspondence to: Derek A. Applewhite (applewhd@reed.edu).

Abbreviations used: CA, constitutively active; Fog, folded gastrulation; MIST, mesoderm invaginating signal transducer; RN-tre, Related to N-terminus of Tre oncogene; Ssh, slingshot.

© 2020 Platenkamp *et al*. This article is distributed by The American Society for Cell Biology under license from the author(s). Two months after publication it is available to the public under an Attribution–Noncommercial–Share Alike 3.0 Unported Creative Commons License (http://creativecommons.org/licenses/by-nc-sa/3.0).

"ASCB®," "The American Society for Cell Biology®," and "Molecular Biology of the Cell®" are registered trademarks of The American Society for Cell Biology.

vitro (Turbedsky *et al.*, 2005; Ricketson *et al.*, 2010; Vicente-Manzanares and Horwitz, 2010). Ser-19 is the main phosphorylation site; however, phosphorylation of both residues results in increased myosinmotor activity (Umemoto *et al.*, 1989; Vicente-Manzanares *et al.*, 2008; Vicente-Manzanares and Horwitz, 2010; Yuen *et al.*, 2009). While poorly understood, phosphorylation of the heavy chain also plays a role in regulating the formation of bipolar minifilaments (Dulyaninova and Bresnick, 2013). Unlike phosphorylation of Sqh, phosphorylation of several key residues in the C-terminus of the heavy chain is thought to block filament formation (Trotter, 1982; Trotter *et al.*, 1985; Barylko *et al.*, 1986). NMII-generated contractility is integrated into the cell signaling machinery mainly through this phosphorylation.

Several signaling pathways converge on the phosphorylation of Sqh, but the Rho pathway most commonly triggers cellular contractility (Chrzanowska-Wodnicka and Burridge, 1996; Wilkinson *et al.*, 2005; Jean *et al.*, 2013). In the Rho pathway, various signals at the cell surface are integrated via G-protein– coupled receptors (GPCRs) that activate guanine nucleotide exchange factors (GEFs) (Barrett *et al.*, 1997; Dawes-Hoang *et al.*, 2005), which in turn catalyze the exchange of GDP for GTP associated with Rho1. Rho1 activates Rho-kinase (Rok) to phosphorylate Sqh dimers bound to the NMII holoenzyme (Morize *et al.*, 1998). Phosphorylated Sqh relieves autoinhibition, allowing for oligomerization and subsequent contractility. In addition, Rok inhibits the protein phosphatase (PP1) complex by way of the myosin-binding subunit (Mbs), resulting in more phosphorylated Sqh (Kimura *et al.*, 1996). Coordination of Rok, other kinases, and phosphatases is essential for proper spatiotemporal regulation of NMII.

While decades of research have elucidated multiple signaling pathways beyond Rho that lead to NMII contractility, there are still large gaps in our understanding of all of the players involved. For example, a recent study using a CRISPR-CAS9 phosphoproteomic approach uncovered previously unidentified cytoplasmic and nuclear phosphorylation targets of myosin light chain kinase (MLCK), indicating that the kinase has a broader role than previously thought (Isobe *et al.*, 2020). In the same vein, the Rac1-GEF STEF was recently shown to regulate Rac1 activity at the nuclear membrane during formation of the nuclear actin cap, an actin-dense contractile structure that interfaces with the nuclear envelope during cell polarization and migration. STEF colocalized with NMIIB (mammals express three isoforms of NMII: A, B, and C) at the actin cap, and down-regulation of STEF decreased NMII contractility (Woroniuk *et al.*, 2018). Furthermore, West-Foyle and colleagues (2018) recently showed that 14-3-3 proteins function as a NMII buffer capable of binding all three mammalian NMII isoforms. Their research suggests that this interaction is evolutionarily conserved and adds a novel layer of complexity to regulation of NMII activation and assembly (West-Foyle *et al.*, 2018). Collectively, these studies suggest that our list of NMII regulators remains incomplete. To uncover novel proteins that regulate NMII, we knocked down a curated set of candidates using a *Drosophila melanogaster* S2 cell line coexpressing a Sqh-EGFP (enhanced green fluorescent protein) fusion protein and mCherry-Actin and looked for changes in NMII localization or dynamics. This screen yielded a single hit, RN-tre (Related to N-terminus of Tre oncogene) (see *Results*).

RN-tre is a known Rab-specific GTPase-activating protein (Rab GAP) with a Tre2-Bub2-Cdc16 (TBC) domain that was previously shown to catalyze the hydrolysis of GTP in *Drosophila* Rabs 5, 6, and 19, which correspond to human Rabs 5, 41, and 43, respectively (Haas *et al.*, 2005, 2007; Ishibashi *et al.*, 2009; Laflamme *et al.*, 2012; Palamidessi *et al.*, 2013). Through these Rabs, RN-tre regulates border cell migration, focal adhesion remodeling, apical localization of R-cell nuclei, macropinocytosis, transferrin and epidermal growth factor internalization, and retrograde transport from the endocytic pathway into the Golgi (Lanzetti *et al.*, 2004; Haas *et al.*, 2005, 2007; Houalla *et al.*, 2010; Frasa *et al.*, 2012; Laflamme *et al.*, 2012; Palamidessi *et al.*, 2013).

Rab proteins (and closely related Arfs) are a subfamily of the Ras GTPases, which encompass 60 human proteins and 29 *Drosophila* proteins, all of which have a regulatory role in intracellular transport. In this role Rabs and Arfs often intersect with the cytoskeleton, most often acting as effectors of motor proteins either by directly recruiting them to vesicles and organelles or indirectly through the recruitment of their adaptors (Kjos *et al.*, 2018; Tanna *et al.*, 2019). One of the best characterized examples is Rab7a, which recruits the dynein–dynactin complex to late endosomes, facilitating retrograde transport of these vesicles (Cantalupo *et al.*, 2001; Jordens *et al.*, 2001; McKenney *et al.*, 2014). Several Rabs also interact with the kinesin family of motor proteins including Rab1, Rab4, Rab5, Rab6, Rab11, and Rab14 just to name a few (Echard *et al.*, 1998; Christoforidis *et al.*, 1999; Jordens *et al.*, 2001; Imamura *et al.*, 2003; Hoepfner *et al.*, 2005; Schlager *et al.*, 2010; Mukhopadhyay *et al.*, 2011, 2014; Ueno *et al.*, 2011; Lee *et al.*, 2015). In some cases these same Rabs also recruit dynein, adding to the complexity of Rab–motor protein interactions (Bielli *et al.*, 2001; Huang *et al.*, 2001; Schlager *et al.*, 2010). Exactly how Rabs recruit the correct motor for proper transport is still unclear but it is likely due to integration of several signaling pathways. On the actin side of intracellular transport, several Rabs have been observed interacting with myosins, including class II myosins, class V myosins, which are highly processive and carry out the bulk of intracellular actin-based transport, and class VI myosins, which "walk" toward the pointed end of actin filaments (Cramer, 2000; Hales *et al.*, 2002; Rodriguez and Cheney, 2002; Roland *et al.*, 2007, 2011; Miserey-Lenkei *et al.*, 2010; Hammer and Sellers, 2011; Lindsay *et al.*, 2013; Encarnação *et al.*, 2016). The cross-talk between the cytoskeleton and Rabs and Arfs is not limited to their ability to recruit motor proteins, and there are several examples that highlight their interaction with the actin cytoskeleton through other mechanisms. Arf1 and Arf6 directly regulate the production of phosphatidylinositols through the recruitment of specific kinases (Honda *et al.*, 1999; Jones *et al.*, 2000; Yin and Janmey, 2003; Myers and Casanova, 2008). These Arfs can lead to the formation of phosphatidylinositol 4,5 bisphosphate (PIP_2), which in turn recruits actin nucleation–promoting factors (NPFs) such as Wiskott–Aldrich syndrome protein (WASP) to activate the actin nucleator Arp2/3 complex (Higgs and Pollard, 2000). Arf6 also indirectly regulates actin polymerization through the recruitment of Rac, which recruits another Arp2/3 NPF, WAVE (Cotton *et al.*, 2007; Tahirovic *et al.*, 2010). This cross-talk has also been observed between the cytoskeleton and GEFs and GAPs of Arfs and Rabs. Arf GAP ASAP1 directly binds to NMIIA and regulates myosin-dependent processes, including cell migration and spreading (Chen *et al.*, 2016; Kjos *et al.*, 2018). Additionally, Arf GEFs BIG1 and BIG2 directly interact with and promote myosin light chain dephosphorylation (Le *et al.*, 2013). Similarly, RN-tre has been shown to cross-talk with the actin cytoskeleton. Rab5 signals to the actin cytoskeleton through RN-tre, which coimmunoprecipitated with the actin bundler actinin-4 (Lanzetti *et al.*, 2004; Haas *et al.*, 2005, 2007; Houalla *et al.*, 2010; Laflamme *et al.*, 2012; Palamidessi *et al.*, 2013). It is thought that this signaling pathway facilitates the formation of circular ruffles coincident

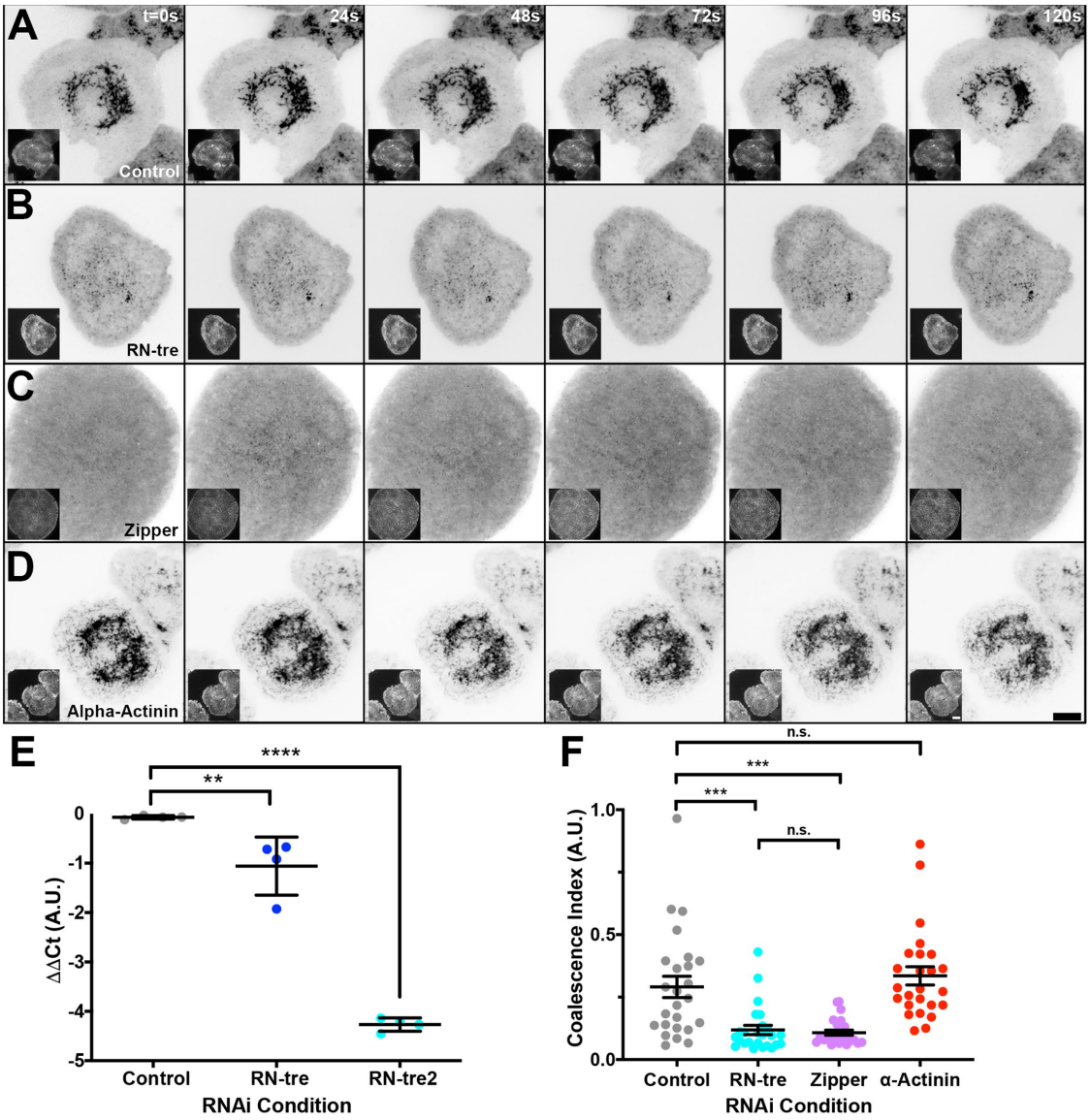

FIGURE 1: RNAi depletion of RN-tre disrupts Sqh localization. (A–D) Live-cell TIRF imaging of S2 cells stably expressing Sqh-EGFP (large images) and Actin-mCH (smaller inset images) at 0, 24, 48, 72, 96, and 120 s. Cells were treated with (A) control, (B) RN-tre target 2, (C) Zipper, or (D) Alpha-Actinin RNAi. Depletion of RN-tre altered the localization of Sqh-EGFP, leading to a decrease in NMII coalescence. (E) RT-qPCR results analyzed by the ΔΔCt method show mRNA levels following treatments with control (gray circles), RN-tre target 1 (blue circles), and RN-tre target 2 (cyan circles) RNAi. There was a statistically significant decrease in the RN-tre mean (± SD) mRNA levels as compared with control RNAi (** p value 0.0078, **** p value < 0.0001, one-way ANOVA with Tukey's post-hoc analysis, $n = 4$). (F) Mean (± SEM) coalescence index measuring the degree of Sqh-EGFP coalescence in cells treated with control (gray circles), Alpha-Actinin (red circles), RN-tre #2 (cyan circles), and Zipper (purple circles) RNAi (n.s. = not statistically significant, *** p value < 0.001, one-way ANOVA test with Tukey's post-hoc analysis, $n = 17–25$). Scale bar is 10 μm.

with the rearrangement of the actin cytoskeleton during receptor tyrosine kinase activation (Lanzetti *et al.*, 2004; Haas *et al.*, 2005, 2007; Houalla *et al.*, 2010; Laflamme *et al.*, 2012; Palamidessi *et al.*, 2013). In this case RN-tre can function as both a GAP for Rab5 and an effector. While cross-talk between RN-tre and the cytoskeleton has been established, our results uncover yet another Rab5-independent mechanism. We identified a role for RN-tre in the regulation of the Rho-signaling pathway and show that depletion of RN-tre decreases the amount of active Rho, which in turn leads to a disruption in NMII localization and a decrease in NMII contractility. Furthermore, we find that this regulation is only partially dependent on RN-tre's GAP activity.

RESULTS

Depletion of RN-tre disrupts nonmuscle myosin II coalescence

In *Drosophila* S2 cells, NMII puncta first appear in the circumferential lamellipodia and undergo a retrograde flow toward the cell center. As these puncta flow into the lamellar region, they coalesce into higher-ordered assemblies, taking up a lamellar, perinuclear position (Rogers *et al.*, 2004; Uehara *et al.*, 2010) (Figure 1A; Supplemental Movie 1). Using total internal reflection fluorescence (TIRF) microscopy, we performed a targeted RNA interference (RNAi) screen in live S2 cells stably expressing EGFP-tagged Sqh under its native promoter and mCherry-tagged actin under the control of a

metallothionein promoter (pMT). The goal of this screen was to identify proteins that potentially regulate NMII, with our initial readout being any changes to its localization or dynamics. Approximately 30 candidates were selected, representing a curated list of proteins that the literature suggests may interact with or regulate NMII but were not previously examined in this context. Our negative control was double-stranded RNA (dsRNA) that targets the bacterial cloning plasmid pBluescript SK, which lacks homology to any gene in the *Drosophila* genome (Rogers and Rogers, 2005), while our positive control for this screen was Rho1 dsRNA as it is a known regulator of the NMII filament assembly (Kimura *et al*., 1996; Somlyo and Somlyo, 2000). We use the same negative control dsRNA throughout the rest of this article unless otherwise noted. This screen yielded a single hit, the Rab GAP RN-tre. In cells depleted of RN-tre, NMII puncta appeared in the lamellipodium, but as they underwent retrograde flow they failed to coalesce into the NMII filament assemblies and instead appeared diffuse throughout the cytoplasm (Figure 1B; Supplemental Movie 1). NMII assembles into diffraction-limited bipolar filaments. Given the limits of our microscope we cannot determine whether these puncta represent these diffraction-limited bipolar filaments. The phenomenon we are reporting here is inhibition of higher-ordered actomyosin filament assemblies that are the result of RN-tre depletion. We generated a second, independent, dsRNA to target RN-tre and observed the same diffuse phenotype. We similarly knocked down the myosin heavy chain Zipper and Alpha-Actinin, a known interactor with RN-tre (Figure 1, C and D). To confirm the efficacy of our RNAi, we performed real-time quantitative-PCR (RT-qPCR) on cells treated with two independent RN-tre targets or control dsRNA and compared the fold decrease in RN-tre mRNA between conditions (Figure 1E). These results indicate that both RN-tre RNAi targets effectively deplete the cells of RN-tre; however, the second RN-tre dsRNA target led to a greater degree of depletion, so we used this target for the majority of the experiments that followed.

To quantify the change in NMII dynamics that we observed in RN-tre–depleted cells, we generated a coalescence index by measuring the relative standard deviation (also known as the coefficient of variation) of fluorescence intensity across the entire cell and dividing this value by the mean pixel intensity (Pearson, 1900; Bouchier-Hayes *et al*., 2008) (Figure 1F). Thus, a high coalescence index is an indicator of a higher degree of NMII filament assemblies, and a low coalescence index is indicative of a more punctate phenotype. By this measurement, we found that depletion of RN-tre led to a statistically significant decrease in the coalescence index as compared with control RNAi-treated samples (p value > 0.001, ordinary one-way analysis of variance [ANOVA], $n = 25$ cells per condition) (Figure 1F). In fact, the loss of coalescence we observed in RN-tre–depleted cells was similar to that of cells depleted of Zipper (Figure 1, C and F). Alpha-Actinin is critical to establishing the sarcomere-like arrangement of NMII in contractile networks, and it has been previously shown that RN-tre interacts with Alpha-Actinin in mammalian cells (Lanzetti *et al*., 2004). Depletion of Alpha-Actinin led a coalescence index that was statistically indistinguishable from control RNAi-treated cells, suggesting that RN-tre's effect on NMII organization is likely independent of this bundler (Figure 1, D and F). Furthermore, we coexpressed mCherry-tagged Alpha-Actinin with EGFP-tagged RN-tre in S2 cells and imaged them by TIRF microscopy and did not observe colocalization between these proteins (Supplemental Figure 1A). Similarly, we failed to observe any substantial colocalization between EGFP-RN-tre and mCherry-Sqh by TIRF or confocal microscopy. suggesting that RN-tre's regulation of NMII localization may be through an indirect mechanism (Supplemental Figure 1, B and C).

To confirm that results from our coalescence index were not an artifact of expression of GFP-tagged Sqh, we performed a similar analysis on S2R+ cells expressing EGFP-tagged cytoplasmic tropomyosin (cTM), another actin bundler coincident with NMII bundles. Depletion of Rho1, Zipper, and RN-tre all led to a similar, statistically indistinguishable decrease in the coalescence index as compared with control RNAi-treated cells, suggesting a similar disruption of the NMII contractile network and corroborating our data gathered from cells expressing Sqh-EGFP (Supplemental Figure 2, A–E).

As the depletions of Zipper and RN-tre were indistinguishable by our coalescence index (Figure 1, B, C, and F), it is possible that depletion of RN-tre also leads to a reduction in NMII levels. Unfortunately, there are no commercially available antibodies against any of the proteins that make up the *Drosophila* NMII holoenzyme. We tried several of the mammalian antibodies that are reported to cross-react with *Drosophila* NMII but failed to observe any staining by immunofluorescence or detection by immunoblot. In lieu of an antibody against endogenous *Drosophila* NMII, we used a stable S2R+ cell line that expresses EGFP-tagged Sqh (*S2R+ Sqh::Sqh-EGFP*) and treated the cells with RNAi targeting RN-tre, Sqh, Zipper, Rho1, and control (Supplemental Figure 2F). Using whole cell lysates made from these cells we performed an immunoblot using an antibody against EGFP (Supplemental Figure 2F). While we did not observe a decrease in EGFP-Sqh levels in cells treated with control, RN-tre, or Rho1 RNAi, depletion of Sqh did lead to a decrease in EGFP-Sqh levels as expected (Supplemental Figure 2, F and G). RNAi depletion of Zipper also led to a slight decrease in Sqh levels, suggesting that there may be some regulatory feedback mechanism between the heavy chain and the regulatory light chain (Supplemental Figure 2, F and G). These results suggest RN-tre is likely not reducing NMII levels, and thus the phenotype we observe following its depletion is through some other mechanism.

RN-tre cross-talks with the Rho1 GTPase pathway

Given the critical role Rho1 signaling plays in the regulation of NMII-generated contractility, we decided to test whether RN-tre is interacting with this pathway as well. Using S2R+ *Psqh::EGFP-Sqh* cells, we depleted Rho1, Rok, RhoGEF2, and Diaphanous (Dia) by RNAi. In cells depleted of Rho1, Rok, RhoGEF2, and Dia, we observed a loss in NMII coalescence and the appearance of NMII puncta statistically indistinguishable from what we observed in RN-tre–depleted cells (p value < 0.0001, one-way ANOVA with Tukey's post-hoc test, $N = 2$, $n = 34$–40 cells) (Figure 2). It should be noted that we cannot exclude the possibility that the activity of the other Rho family GTPases, Rac and Cdc42, is not perturbed as a result of Rho1 depletion as they all compete for binding to RhoGDI. Unlike Rho1 or Rok depletion, RN-tre depletion does not lead to cytokinesis defects, suggesting that RN-tre's role in regulating the NMII dynamics is restricted to interphase.

To further probe the Rho1 pathway, we attempted to rescue NMII coalescence in RN-tre–depleted cells by expressing constitutively active (CA) forms of proteins in the Rho1 pathway. We treated the S2R+ *Psqh::EGFP-Sqh* cells with RN-tre or control RNAi and transfected cells with mCherry-Gap43 as a negative control or with a dual expression vector that expresses mCherry-Gap43 and untagged CA $Rho1^{14V}$ (RhoCA) (Dorsten *et al*., 2007) (Figure 3, A–D). Expression of Rho1CA restored the coalescence of NMII observed in RN-tre RNAi-treated cells to the same extent as in control RNAi-treated cells, and higher-ordered NMII filament assemblies once again formed in the perinuclear regions of the cells (Figure 3D). Similarly, we treated

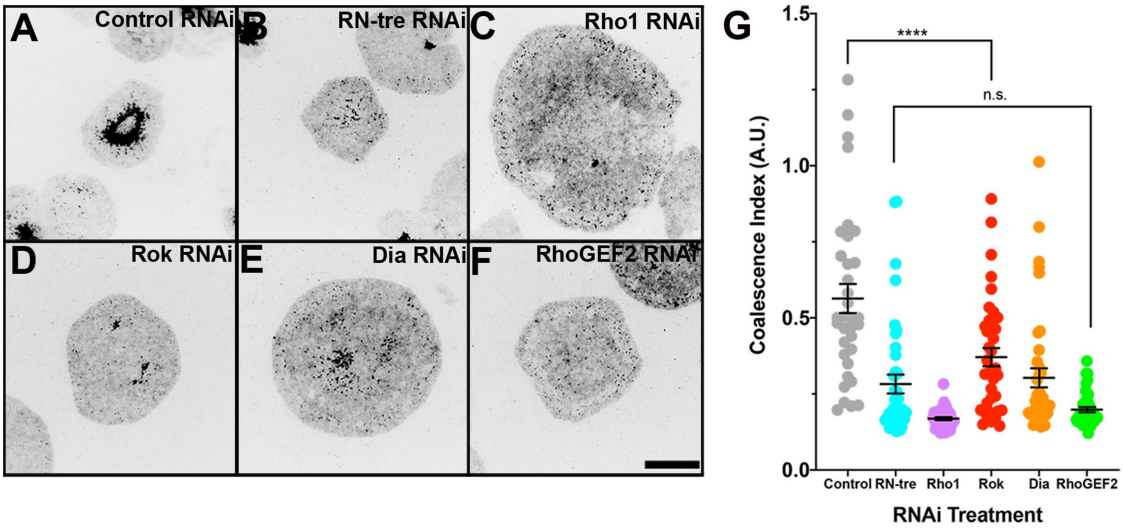

FIGURE 2: Depletion of RN-tre phenocopies RNAi depletion of proteins in the Rho1 signaling pathway. S2R+ cells stably expressing Sqh-EGFP were treated with (A) control, (B) RN-tre #3, (C) Rho1, (D) Rok, (E) Dia, or (F) RhoGEF2 RNAi. RN-tre depletion leads to a similar punctate phenotype as depletion of proteins in the Rho1 signaling pathway. Scale bar is 10 μm. (G) Coalescence index following treatment with control (gray circles), RN-tre #3 (cyan circles), Rho1 (purple circles), Rok (red circles), Dia (orange circles), and RhoGEF2 (green circles) RNAi. The mean (± SEM) coalescence index of cells treated with control RNAi was statistically significantly different from all other RNAi treatments (**** p value < 0.0001, one-way ANOVA with Tukey's post-hoc test, $n = 20$ cells per condition, $N = 2$), while RNAi depletion of RN-tre was not statistically significantly different from Rho1, Rok, RhoGEF2, or Dia.

S2R+ *Psqh::EGFP-Sqh* cells with RN-tre or control RNAi and transfected them with the CA N-terminal kinase region (residues 1–530) of Myc-tagged Rok (RokCA) (Verdier *et al.*, 2006) under the control of metallothionein promoter (Figure 3, E–H). Expression of RokCA was also able to restore the organization of NMII filament assembly to the same extent as control RNAi-treated cells (Figure 3H). In the context of NMII dynamics during interphase specifically, RN-tre depletion appears to phenocopy depletion of proteins in the Rho1 pathway.

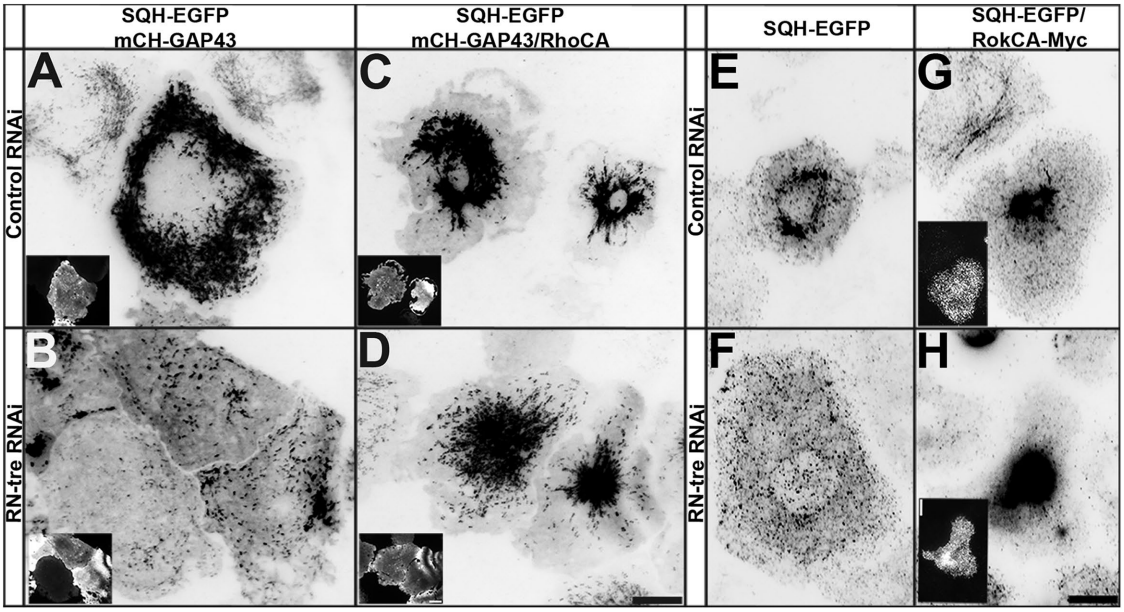

FIGURE 3: Loss of NMII coalescence following RN-tre depletion can be rescued by expression of CA proteins in the Rho1 pathway. (A–D) Live, stable S2R+ cells, expressing Sqh-EGFP and transiently expressing (A, B) mCherry-GAP43 (inset at lower magnification) or (C, D) mCherry-GAP43 (inset at lower magnification) and untagged, CA Rho1 (RhoCA) from a dual expression vector. Cells were treated with control RNAi (A, C) or RN-tre #1 RNAi (B, D). Expression of RhoCA rescued the loss of NMII coalescence that results from RN-tre depletion (D). (E–H) Fixed S2R+ stable cells expressing Sqh-EGFP alone (E, F) or Sqh-EGFP and CA Myc-tagged Rok (anti-Myc staining shown in lower magnification) (G, H). Cells were also treated with either control RNAi (E, G) or RN-tre #1 RNAi (F, H). Expression of RokCA-Myc also rescues the loss of NMII coalescence that results from RN-tre depletion. Scale bars are 10 μm.

Furthermore, overexpression of CA proteins in the Rho1 pathway can rescue the loss of coalescence that occurs upon RN-tre depletion.

We next turned our attention to the phosphorylation state of Sqh. Activation of Rho1 signaling leads to the phosphorylation of Sqh and subsequent activation. Thus, we investigated the possibility that RN-tre depletion inhibits Sqh phosphorylation, trapping NMII in its closed conformation and rendering it unable to oligomerize. We tested this possibility by treating cells with control, RN-tre, Rho1, or two different dsRNAs targeting Rok and immunostained them using an antibody raised against a synthetic phosphopeptide corresponding to residues surrounding Ser-19 of human myosin RLC. This antibody cross-reacts with the *Drosophila* RLC, Sqh (Figure 4, A–E). We counted the cells that were positive for phosphoserine under these five conditions and found that depletion of RN-tre led to a significant decrease in the number of phosphomyosin-positive cells as compared with control RNAi-treated cells (p value > 0.0001, N = 2–5, n = 600 cells, one-way ANOVA with Tukey's post-hoc test) (Figure 4F). In fact, depletion of RN-tre was statistically indistinguishable from depletion of either Rok RNAi conditions. While other kinases are known to phosphorylate Sqh, Rok is thought to be the main kinase (Dawes-Hoang *et al*., 2005).

The decrease in phosphomyosin staining we observed following depletion of RN-tre suggests a disruption in events upstream of Rok activation. One of the first regulatory steps in Rho signaling is the loading of Rho1 with GTP, so we turned our focus to this event. We treated S2R+ cells with control or RN-tre RNAi and performed an active Rho1 pull-down assay using the Rho1-binding domain of Rhotekin, which preferentially binds active Rho1 (Reid *et al*., 1996) (Figure 4G). We included control lysates treated with excess GDP to trap Rho1 in the "off" state and lysates treated with GTPγS, a slowly hydrolyzed form, which traps Rho1 in the "on" state. Depletion of RN-tre led to a statistically significant decrease in the amount of active Rho1 in our pull down compared with control RNAi-treated cells, with the amount being similar to that of Rho1-GDP (p value = 0.0461, Student's t test, N = 3) (Figure 4H). Not only would less active Rho1 lead to a decrease in phosphorylated Sqh, but it would also lead to less active Diaphanous (Afshar *et al*., 2000; Kato *et al*., 2001; Homem and Peifer, 2008; Rousso *et al*., 2013; Abreu-Blanco *et al*., 2014), which is thought to nucleate the unbranched actin filaments needed to form the contractile network.

RN-tre depletion inhibits NMII contractility

RN-tre depletion appears to disrupt NMII localization and dynamics through Rho1 signaling; however, it is unclear whether this loss in coalescence is also associated with a change in NMII contractility. To test RN-tre's role in regulating NMII contractility, we turned to the Folded-gastrulation (Fog) pathway (Leptin and Grunewald, 1990; Dawes-Hoang *et al*., 2005; Leptin, 2005; Manning and Rogers, 2014; Martin and Goldstein, 2014). During *Drosophila* gastrulation, activation of the Fog pathway leads to signaling cascade converging on Rho1 activation and subsequent apical constriction generated by NMII contractility (Parks and Wieschaus, 1991; Costa *et al*., 1994; Barrett *et al*., 1997; Peters and Rogers, 2013; Manning and Rogers, 2014; Vasquez *et al*., 2014; Kerridge *et al*., 2016; Xie *et al*., 2016; Jha *et al*., 2018). This pathway may be recapitulated in *Drosophila* S2R+ cells; when perfused with exogenous recombinant Fog-Myc (from S2: Fog-Myc cells), S2R+ cells undergo a stereotypical contraction coincident with phase-dark and phase-light ruffles visible by phase-contrast microscopy (Manning *et al*., 2013; Manning and Rogers, 2014; Peters and Rogers, 2013; Peters *et al*., 2018) (Figure 5, A and B). We treated S2R+ cells with RNAi targeting RN-tre, Rho, and control, applied concentrated Fog-Myc media or control media, and counted the cells that underwent constriction (Figure 5, A–F). As expected, Rho depletion significantly reduced the number of cells that respond to Fog. Similarly, we observed a statistically significant decrease in the fraction of cells responding to Fog following RN-tre RNAi as compared with control (p value < 0.01, N = 3, n = 154–166 cells per condition, one-way ANOVA with Tukey's post-hoc test), indicating that either Fog signaling is interrupted by RN-tre depletion or NMII contractility is inhibited (Figure 5G).

Given its role in regulating several different Rabs, RN-tre depletion could be preventing the proper transport of the mesoderm invaginating signal transducer (MIST) receptor to the cell membrane, thus disrupting the Fog signaling pathway. To test this possibility, we treated cells expressing EGFP-tagged MIST and mCherry-tagged Gap43 with control, RN-tre, or Rho1 RNAi and imaged the surface localization of both proteins via TIRF microscopy (Supplemental Figure 3). There was no difference between the ratio of MIST-EGFP to mCH-Gap43 average signal intensity at the cell surface, suggesting that the reduction in cellular contractility is not a consequence of aberrant cellular receptor transport.

To get a better understanding of how RN-tre depletion prevented Fog-induced cellular contractility, we performed the assay using live S2R+ *Psqh::EGFP-Sqh* cells and imaged them by TIRF microscopy (Figure 6, A–C). S2 cells lack the coreceptors MIST and Smog and therefore cannot respond to Fog (Manning *et al*., 2013). Upon perfusion of Fog on control cells, we observed an initial wave of NMII filament assembly in the periphery. These filaments flowed centripetally to take up a perinuclear position (Figure 6A; Supplemental Movie 2). When we quantified the assembly of NMII filaments over time using our coalescence index, we first observed a decrease in coalescence followed by a steady increase corresponding to formation of perinuclear filament oligomers in control cells (Figure 6D). In RN-tre RNAi-treated cells the same initial wave occurred in the periphery of the cells but the network failed to flow inward and remained loosely organized (Figure 6B; Supplemental Movie 2). Similarly, when we performed this live assay on Rho1 RNAi-treated cells, we observed an initial wave of NMII dynamics but failed to observe the subsequent assembly of filaments (Figure 6C; Supplemental Movie 2). Our coalescence index tracked these dynamics in RN-tre or Rho1 RNAi-treated cells, revealing that there was no increase in coalescence to the degree of control cell coalescence following Fog perfusion (Figure 6D).

While Fog signaling represents a signaling cascade that triggers an acute morphogenetic restructuring of epithelial tissues, we wanted to determine whether RN-tre regulates contractility in additional contexts. Actin retrograde flow is the result of two processes, the force of the cell membrane pushing back against polymerizing actin filaments and NMII contractility. Inhibition of NMII through pharmaceutical means or by RNAi leads to increases in cell protrusiveness and the rates of actin retrograde flow in the lamellipodium (Cai *et al*., 2006; Even-Ram *et al*., 2007; Vicente-Manzanares *et al*., 2009). To track actin retrograde flow in *Drosophila* S2 cells, we capitalized on the heterogeneous incorporation of the fluorescent actin that results from expressing low levels of fluorescently tagged actin. The resulting fiducial marks, when tracked by kymography, can be used to obtain rates of actin retrograde flow (Waterman-Storer *et al*., 1998). We treated cells expressing low levels of EGFP-tagged actin with RNAi targeting RN-tre, slingshot (Ssh) the cofilin phosphatase, and control (Figure 7, A–C). Ssh depletion was previously shown to inhibit the rate of actin retrograde flow (Iwasa and Mullins, 2007) and as expected, Ssh depletion led to a significantly slower rate of actin retrograde flow (Figure 7, C and D). This analysis also

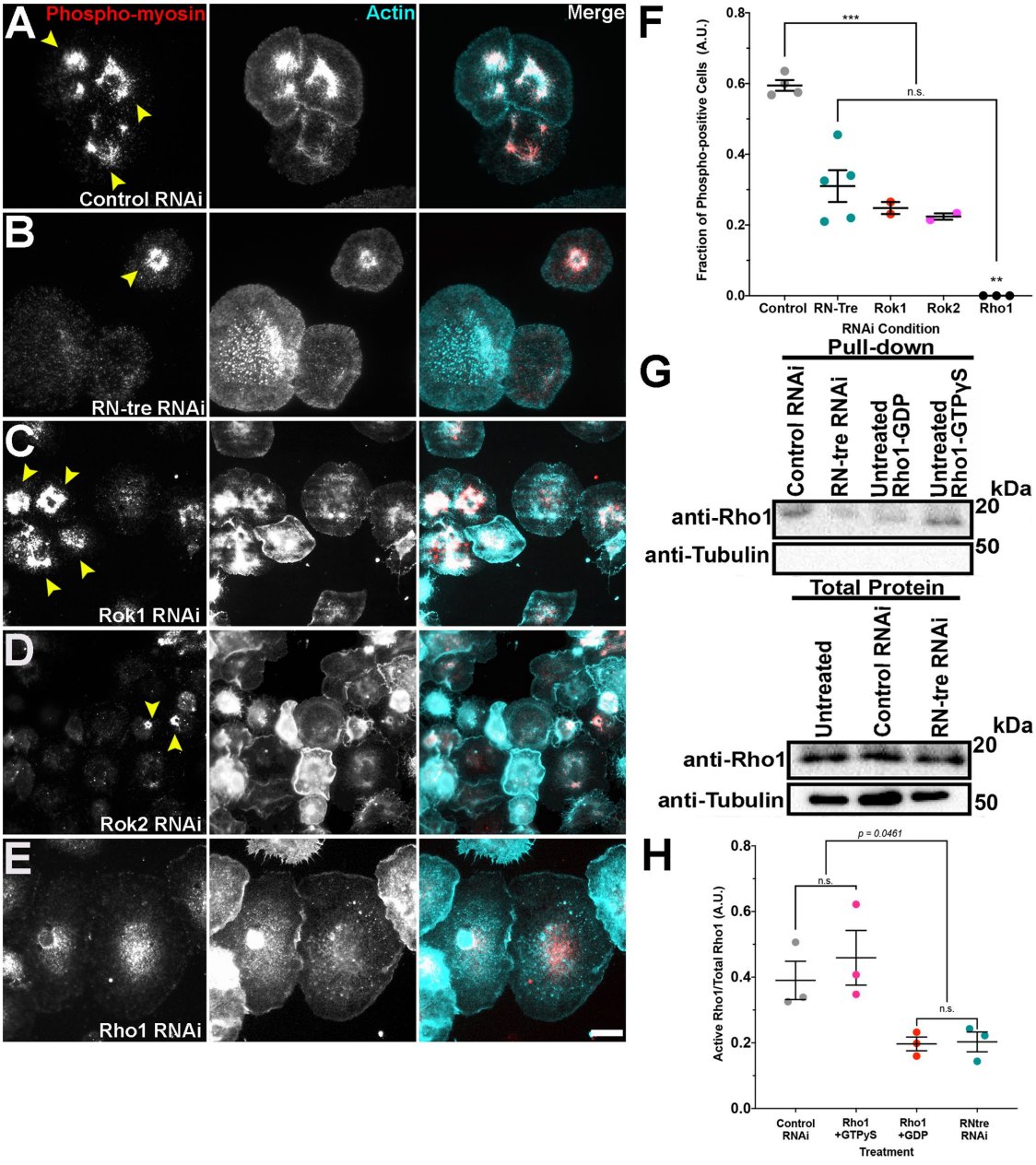

FIGURE 4: Depletion of RN-tre inhibits the phosphorylation of the NM II regulatory light chain and decreases the amount of active Rho1. S2R+ cells fixed and stained for anti-phosphomyosin (red in merge) and F-actin (cyan in merge) following treatment with (A) control RNAi, (B) RN-tre #2 RNAi, (C) Rok1 RNAi, (D) Rok2 RNAi, or (E) Rho1 RNAi. (Note that the phosphomyosin staining in the Rho1 RNAi condition is diffuse and ill-defined, indicative of nonspecific background staining and not an actual signal.) Yellow arrowheads in A–E indicate cells with prominent phosphomyosin staining. Scale bar is 10 μm. (F) Quantification of the number of phosphomyosin-positive cells following RNAi treatment with control (gray circles), RN-tre #2 (cyan circles), two independent Rok targets (red and magenta circles), and Rho1 (black circles). RNAi depletion of RN-tre led to a statistically significant decrease in the mean (± SEM) number of phosphomyosin-positive cells as compared with control RNAi-treated cells (*** p value < 0.0001, two-way ANOVA with Tukey's post-hoc analysis, $n = 200$ cells, $N = 3$); however, depletion of RN-tre was not statistically significantly different from Rok RNAi depletion. The number of phosphomyosin-positive cells following Rho1 RNAi was statistically different from control, Rok, and RN-tre RNAi. (G) Western blots of Rho1 and β-tubulin in whole cell lysate (total protein) and pull-down samples. Cells were treated with control RNAi, RN-tre #2 RNAi, or untreated. The untreated lysates were preincubated with GDP or GTPγS as controls. (H) Quantification of Rho1 Western blot following active-Rho1 pull down. β-Tubulin was used for normalization, and then the ratios of active Rho1 over total Rho1 were calculated for control RNAi, Rho1-GTPγS, Rho1-GDP, and RN-tre #2 RNAi (mean ± SEM) (Student's t test, p value = 0.0461, $N = 3$).

revealed that RN-tre depletion led to a significantly faster rate of actin retrograde flow when compared with Ssh and control RNAi-treated cells (one-way ANOVA, p value = 0.0085, one-way ANOVA, n = 60–80 speckles per RNAi condition, N = 3), indicative of an inhibition of NMII function (Figure 7, B and D). Furthermore, this increase in actin retrograde flow does not appear to come at the

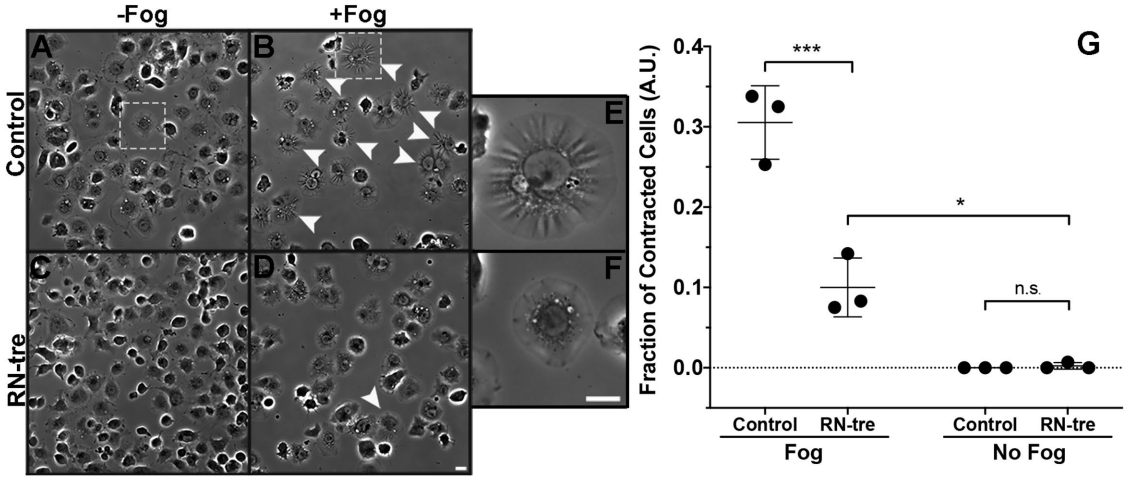

FIGURE 5: RN-tre depletion inhibits Fog-stimulated NM II contractility. S2R+ cells treated with control RNAi (A, B) or RN-tre #2 RNAi (C, D) were then incubated with control media (A, C) or Fog-conditioned media (B, D) and imaged by phase-contrast microscopy. White arrowheads indicate contracted cells. (E) Larger image of constricted cell from B. (F) Larger image of relaxed cell from A. (G) The fraction of contracted cells to total cells was determined for each condition (control and RN-tre #2 RNAi with control media and Fog-conditioned media). Shown is the mean with SD. Significantly more cells contracted when perfused with Fog-conditioned media in both RNAi conditions as compared with control media (No Fog). Upon the perfusion of Fog-conditioned media, significantly fewer RN-tre #2 RNAi-treated cells contracted as compared with control RNAi-treated cells (mean ± SD) (* p value 0.0213, *** p value < 0.001, two-way ANOVA with Tukey's post-hoc analysis, n = 154–166 cells, N = 3 independent experiments). Scale bars are 10 μm.

expense of the integrity of the overall actin cytoskeleton as we did not observe any gross morphological differences between control and RN-tre–depleted cells expressing mCherry-Actin (Supplemental Figure 4, A–D). Collectively, we have demonstrated by two different assays that depletion of RN-tre inhibits NMII contractility. These results suggest that RN-tre has a more general role in the regulation of NMII contractility.

RN-tre's GAP activity is partially required for its role in the regulation of NMII filament contractility

RN-tre is characterized by a TBC domain that promotes GTP hydrolysis through the dual arginine finger mechanism common in Ras GAPs (Lanzetti *et al.*, 2000). RN-tre has been shown to function as a GAP for Rabs 5, 41, and 43, which correspond to *Drosophila* Rabs 5, 6, and 19, respectively (Lanzetti *et al.*, 2000, 2004; Haas *et al.*, 2005, 2007). Given its role as a GAP, RN-tre depletion could lead to hyperactivation of one of these Rabs. To test this hypothesis, we overexpressed CA *Drosophila* Rab5, Rab6, and Rab19 and imaged the localization and dynamics of RLC (Supplemental Figure 5, A–D). Overexpression of any of these CA Rabs did not alter NMII dynamics. Furthermore, neither RNAi depletion nor overexpression of the dominant negative (DN) version of these Rabs perturbed NMII localization or dynamics (Supplemental Figure 5, A and E–K). These results suggest that RN-tre's role in regulating NMII localization and dynamics is independent of its established role in Rab signaling.

To more directly test whether RN-tre's GAP activity is required for its role in regulating NMII, we mutated the conserved catalytic arginine finger motif common on Ras GAPs and then tested whether this version of RN-tre could rescue Sqh phosphorylation. We generated two stable S2R+ cell lines that express either wild-type RN-tre or RN-tre mutated at the catalytic arginine residue (R153A, GAP-dead), both with divergent genetic sequences at the wobble position, making them refractory to one of our RN-tre dsRNAs (Endo-RN-tre) while remaining sensitive to another RN-tre dsRNA (All-RN-tre), which we confirmed by Western blot (Figure 8, A–H). Following treatment with control and these two different RN-tre dsRNAs, we fixed and stained the cells for phosphomyosin. We also prepared whole cell lysates from these cells to confirm the expression of our Myc-tagged RN-tre constructs. Unfortunately, the expression levels varied greatly between stable cell lines, so we normalized our phosphomyosin quantification to the control RNAi treatment for each cell line (Figure 8, G and H). Wild-type RN-tre expression fully rescued phosphomyosin staining; however expression of the GAP-dead mutant resulted in only a partial rescue (p value < 0.0001, one-way ANOVA with Tukey's post-hoc test, N = 2, n = 159–167 cells per round) (Figure 8H). This finding suggests that RN-tre's GAP activity is not fully required to restore phosphomyosin staining and thus NMII contractility and indicates GAP-independent function for RN-tre in regulating Rho signaling. GAP-dead RN-tre was not mislocalized; coexpression of mCherry-RN-tre and EGFP-RN-tre (R153A) in S2R+ cells revealed no differences in localization between these two constructs (Figure 8, I and J).

DISCUSSION

In *Drosophila* S2 and S2R+ cells, NMII forms a perinuclear contractile network from individual NMII motor proteins that, upon phosphorylation, oligomerize forming larger bipolar assemblies that bind to antiparallel arrays of actin filaments. The ATP-dependent sliding of these filaments as the NMII heads "walk" along actin can lead to the generation of force needed for several NMII-dependent cellular functions including cell shape change that occurs during development of tissues and organs, the formation of cell–cell and cell–matrix adhesions, cytokinesis, and cell motility (Vicente-Manzanares *et al.*, 2009). In nonmuscle cells, the critical point of regulation is the phosphorylation of the regulatory light chain, and without this post-translational modification individual NMII molecules remain trapped in an autoinhibited conformation, failing to form the larger bipolar filament assemblies (Scholey *et al.*, 1980; Sellers *et al.*, 1981; Trybus, 1989) (Figure 9). It is the phosphorylation of the regulatory light chain by such kinases as citron kinase, myosin light chain kinase, and

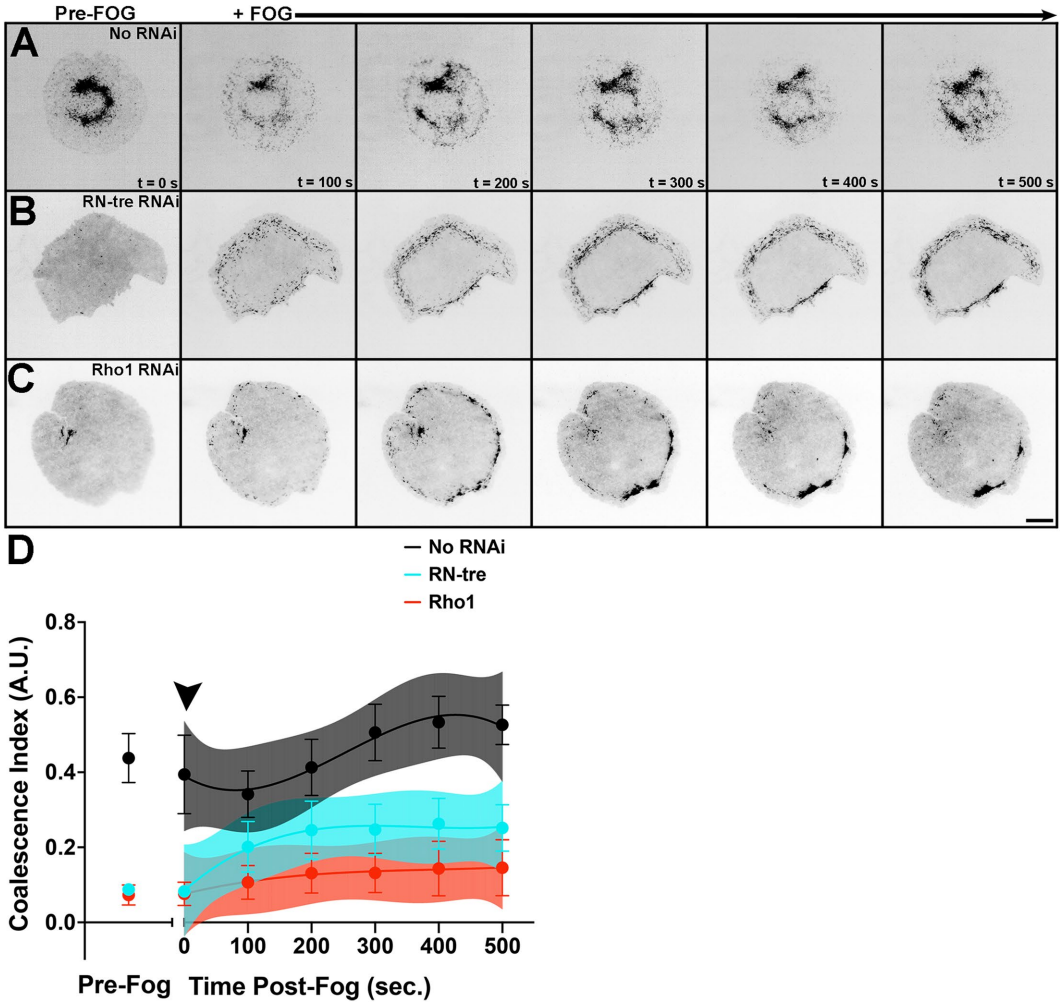

FIGURE 6: RN-tre depletion disrupts NMII localization in Fog-induced contractility. Sqh-EGFP–expressing S2R+ cells were treated with (A) no RNAi, (B) RN-tre #2 RNAi, or (C) Rho1 RNAi and then perfused with Fog-conditioned media during live-cell TIRF imaging. Pre-Fog image is given (far left) and shows the distribution of Sqh before the Fog-induced rearrangement. Scale bar is 10 μm. (D) Coalescence index shown over time for no RNAi condition (black), RN-tre #2 RNAi (cyan), and Rho1 RNAi (red). Closed circles represent the mean, error bars represent the SEM (n = 4–6 cells per RNAi condition), and the shaded region is a regression fit with the 95% confidence interval. The arrowhead denotes the time when Fog was added to the cells. Depletion of RN-tre and Rho1 prevented the formation of a perinuclear contractile network.

Rok that relieves this inhibition (Amano *et al.*, 1996; Tan *et al.*, 2003; Yamashiro *et al.*, 2003), while the phosphatase activity of PP1 complex maintains NMII in a closed conformation (Figure 9). It is this phosphorylation/dephosphorylation cycle that contributes to both the spatial and temporal regulation of contractility (Tan *et al.*, 2003; Matsumura and Hartshorne, 2008). Depletion of Rho1, which activates Rok, or depletion of Rok itself results in a characteristic punctate phenotype indicative of this lack of oligomerization. A similar punctate phenotype occurs upon the expression of an alanine-substituted nonphosphorylatable RLC (Dean and Spudich, 2006). Thus, it was surprising to observe a similar punctate phenotype upon the depletion of RN-tre, a Rab GAP (Figure 1). While this punctate phenotype is suggestive of an inhibition of Rho1 signaling to the regulatory light chain, it could also result from aberrant actin organization leaving NMII with no place to bind, a reduction in NMII levels so that oligomers cannot form, inhibition of NMII heavy chain phosphorylation, or an inhibition of the formation of the NMII holoenzyme itself. While not exhaustive of all actin bundlers, depletion of Alpha-Actinin, one of the main actin-binding proteins in contractile networks, failed to recapitulate the punctate phenotype that we observed upon RN-tre depletion (Figure 1). Our results also suggest that depletion of RN-tre does not lead to a reduction in RLC or heavy chain NMII protein levels (Supplemental Figure 2F). Furthermore, a reduction of NMII protein levels or the inhibition of the formation of the NMII holoenzyme itself would likely also result in a failure in cytokinesis, a phenotype that we failed to observe following RN-tre depletion. Phosphorylation of the heavy chain, by kinases such as protein kinase C (PKC) and casein kinase 2 (CK2), is associated with the disassembly of NMII filaments (Rahmsdorf *et al.*, 1978; Kuczmarski and Spudich, 1980; Collins *et al.*, 1982a,b; Heissler and Sellers, 2016). Notably, phosphorylation of the heavy chain by PKC has been shown to be dispensable for viability in flies, suggesting that this interaction may not be critical to NMII filament dynamics in *Drosophila* (Su and Kiehart, 2001). This leaves the RLC as the likely means of regulation. Depletion of RN-tre led to a reduction in the number of cells with phosphorylated RLC that is likely the result of the decrease in the amount of GTP-loaded active Rho1 in cell lysates following RN-tre depletion (Figure 4, A, B, and F). Depletion of

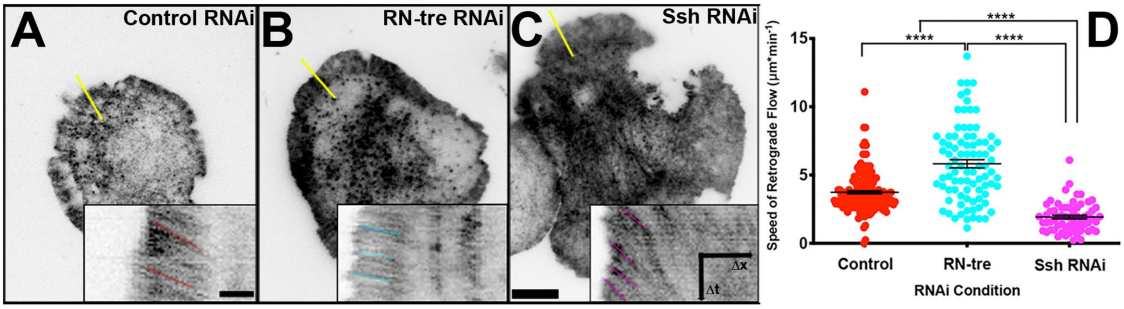

FIGURE 7: RN-tre depletion increases the rate of actin retrograde flow. S2 cells stably expressing mCherry-Actin under the control of the metallothionein promoter were induced with 25–50 μM $CuSO_4$, resulting in actin speckling. Cells were treated with (A) control, (B) RN-tre #1, or (C) slingshot (Ssh) RNAi. The yellow line in each lower-magnification image indicates the lamellipodial region used to generate kymographs shown in each corresponding image at higher magnification (lower right corner). For each kymograph, time is shown on the *y*-axis and distance is on the *x*-axis. The lines in each kymograph are representative actin speckle tracks that were used to calculate the rate of actin retrograde flow. (D) Quantification of the rate of actin retrograde flow following control RNAi (red circles), RN-tre #1 RNAi (cyan circles), and Rho1 (magenta circles). Black bars represent the mean and SEM. Depletion of RN-tre led to a statistically significant increase in mean (5.8 ± 0.3 μm*min^{-1}) actin retrograde flow rate as compared with control RNAi (3.7 ± 0.1 μm*min^{-1}, one-way ANOVA, **** p value < 0.0001, n = 60–170 speckles per RNAi condition, N = 3). Scale bar is 10 μm for the lower-magnification images and 2 μm for the kymographs.

RN-tre also phenocopied some aspects of depletion of other proteins in the Rho1 pathway (Figures 2 and 4, C–F), and the punctate RLC localization phenotype that we observed could be rescued by expression of CA Rho1 and Rok (Figure 3), further indicating cross-talk between RN-tre and the Rho1 signaling pathway. While depletion of RN-tre was statistically indistinguishable from depletion of Rho1, Rok, RhoGEF2, and Dia as per our coalescence assay (Figure 2), our results do not preclude the involvement of other proteins known to interact with the Rho1 pathway. For example, the newly characterized *Drosophila* Rho GEF Dp114 RhoGEF has been shown to play a role in junctional activation of Rho1 in the ectoderm, kinases such as MRCK, citron kinase, and ZIPK have also been shown to phosphorylate the RLC, and other actin-binding and organizing proteins such as Abled and Enabled also play roles in the assembly of actomyosin filaments (Gertler *et al.*, 1995; Fox and Peifer, 2007; Vicente-Manzanares *et al.*, 2009; de las Bayonas *et al.* 2019) (Figure 9). These proteins could function to maintain the actomyosin network to some lesser degree, independent of RN-tre. While interesting, the interaction between RN-tre and these other proteins is beyond the scope of this study. Our results also indicate that RN-tre's GAP activity is only partially required for Rho1 signaling (Figure 8, A–H). It was previously shown that RN-tre can interact with the cytoskeleton in a GAP-independent manner (Lanzetti *et al.*, 2004). Here we have demonstrated that RN-tre cross-talks with the Rho1 signaling pathway, more specifically the phosphorylation of the RLC, which ultimately leads to the regulation of NMII-generated contractility.

Cross-talk between the transport machinery and NMII

Cross-talk between Rabs and Arfs (their GEFs and GAPs) and the cytoskeleton is a well-documented phenomenon. Rabs and Arfs can recruit molecular motor proteins directly or indirectly to facilitate transport, but moreover, these proteins can regulate the cytoskeleton independently of motor proteins (Kjos *et al.*, 2018; Tanna *et al.*, 2019). While not traditionally associated with intracellular transport, cross-talk between Rabs and class II myosins has also been well documented (Miserey-Lenkei *et al.*, 2010; Borg *et al.*, 2014; Vestre *et al.*, 2019). NMII was a positive hit in a yeast two-hybrid screen using Rab7b as bait. This interaction was later confirmed in monocyte-derived dendritic cells, where endogenous Rab7b was able to coimmunoprecipitate with NMII. Even further, Borg and colleagues (2014) demonstrated that a CA variant of Rab7b was able to coimmunoprecipitate substantially more NMII than wild-type Rab7b and that this interaction was likely direct, as bacterially expressed Rab7b was able to interact with the bacterially expressed NMII tail in a purified system. Depletion of Rab7b, among other phenotypes, led to a reduction in stress fiber formation, a decrease in the amount of active RhoA in cell lysates, and a reduction in the amount of phosphorylated RLC (Borg *et al.*, 2014). Similarly, Rab6 has been shown to directly interact with NMII (Miserey-Lenkei *et al.*, 2010). Like Rab7b, depletion of Rab6 also led to a decrease in RLC phosphorylation; however, unlike Rab7b, Rab6 seems to be working through the Rho family GTPase Cdc42 and its GEF Trio (Vestre *et al.*, 2019). Cdc42 activation has been linked to filopodia formation; thus, Rab6 may be regulating filopodia formation through this interaction. For both Rab7b and Rab6, depletion led to a decrease in NMII activation through a reduction in the phosphorylation of the RLC. Depletion of a GAP for either one of these Rabs would theoretically lead to an increase in their activity and a subsequent increase in RLC phosphorylation. We found that neither the overexpression of CA Rab6, overexpression of dominant negative Rab6, nor the depletion of Rab6 led to any changes in NMII localization or dynamics (Supplemental Figure 5, C, F, and J). As there have been no reported links between RN-tre and Rab7b, we did not pursue this further.

Cross-talk between RN-tre and the cytoskeleton

While RN-tre has not been previously associated with NMII, it has been shown to interact with Alpha-Actinin, an actin-bundling protein that organizes F-actin into sarcomere-like contractile networks in nonmuscle cells (Lanzetti *et al.*, 2004). It should be noted that RN-tre is orthologous to the N-terminus of the human Tre2 oncogene. Tre2 was previously found to interact directly with two cytoskeletal proteins, Ankrd44 and the RLC of myosin II, in vitro and in vivo in human HEK-293 cells (Dechamps *et al.*, 2006). While Tre2 colocalizes with RLC in human cells, we did not observe colocalization of RN-tre and RLC in *Drosophila* cells (Supplemental Figure 1). RN-tre coimmunoprecipitated with Alpha-Actinin in a platelet-derived growth factor (PDGF)-dependent manner; however, this interaction is likely indirect as bacterially expressed fragments of Alpha-Actinin and RN-tre failed to interact in vitro. Overexpression of

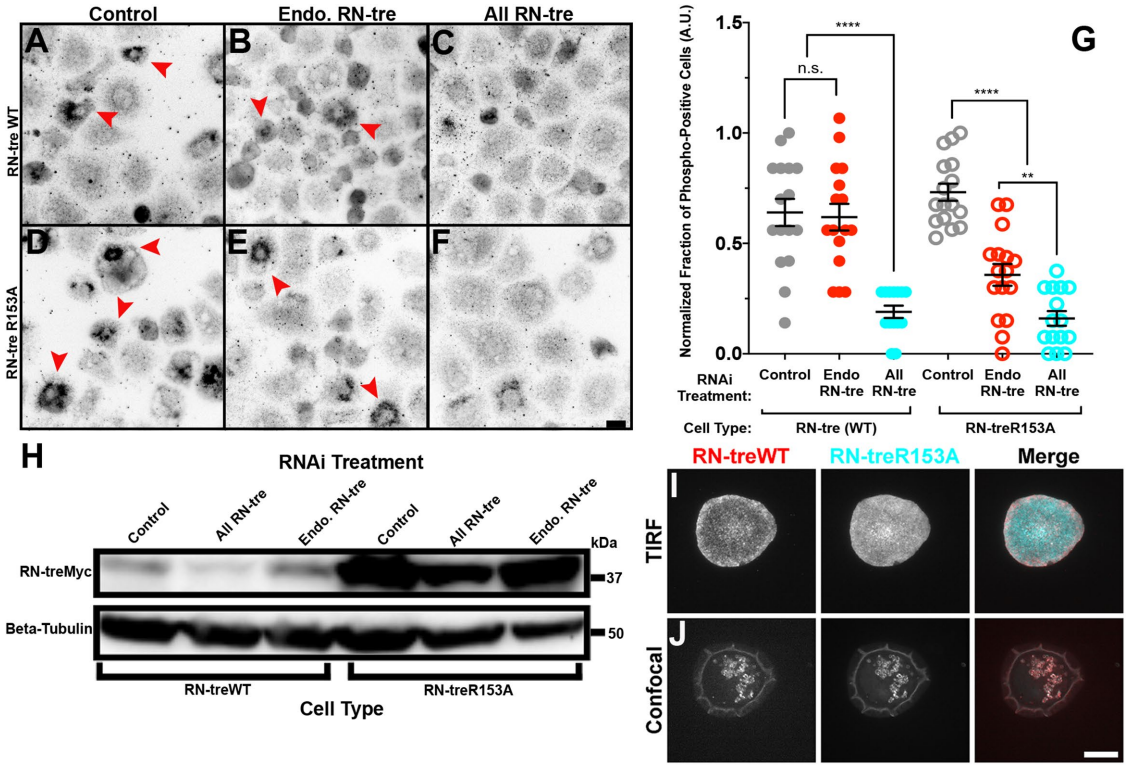

FIGURE 8: RN-tre's GAP activity is partially required for Rho1 signaling. (A–F) S2R+ cells stably expressing a Myc-tagged wild-type RN-tre with nucleotides 1266–1601 mutated at the wobble position (A–C) or expressing a Myc-tagged RN-tre(R153A) with nucleotides 1266–1601 mutated at the wobble position as well as a mutation at the amino acid position 153 (D–F). Both of these constructs are refractory to Endo RN-tre dsRNA but sensitive to All RN-tre #2 dsRNA. Cells were fixed and stained for phosphomyosin; yellow arrowheads indicate phosphomyosin-positive cells. Cells were treated with control RNAi (A, D), All RN-tre #2 RNAi (B, E), or Endogenous RN-tre RNAi (C, F). Scale bar is 10 μm. (G) Quantification of the normalized fraction of phosphomyosin-positive cells following treatment with control RNAi (gray closed and open circles), Endo RN-tre RNAi (red closed and open circles), and All RN-tre #2 RNAi (cyan closed and open circles). The closed circles represent the RN-tre wild-type (WT) cell line, while the open circle represents the RN-tre R153A cell line. The number of phospho-positive cells was normalized to the control RNAi treatment for each cell type to mitigate expression differences (mean ± SEM) (** p value < 0.01, **** p value < 0.0001, one-way ANOVA, $n = 8$ frames, $N = 2$). (H) Western blot for RN-tre (anti-Myc) and β-tubulin following RNAi treatments. Note the differences in expression levels between the two stable cell lines that were consistent throughout experimentation. (I) An S2R+ cell coexpressing mCherry wild-type RN-tre (left, red in merged image) and GAP-dead (R153A) RN-tre (middle, cyan in merged image) imaged by TIRF microscopy. (J) The same cell as in I imaged with confocal microscopy; both wild-type and GAP-dead RN-tre colocalize to the same structures. Scale bar is 10 μm.

RN-tre suppressed PDGF-stimulated ruffles, actin-based structures that form as the result of RTK activation and contain Alpha-Actinin. The suppression of these ruffles, as well as the inhibition of macropinocytosis, was independent of RN-tre's GAP activity as GAP-dead mutants were capable of inhibiting both activities (Lanzetti *et al.*, 2004). Despite its role in organizing the contractile network in nonmuscle cells, depletion of Alpha-Actinin failed to phenocopy the loss of NMII coalescence that we observed following depletion of RN-tre (Figure 1D), which suggests that RN-tre's role in regulating NMII localization and dynamics is independent of its interaction with Alpha-Actinin. Furthermore, RN-tre depletion disrupts the NMII contractile network during interphase or the steady-state and is independent of signaling initiated by factors such as PDGF (Figures 1 and 7).

A role for RN-tre in cell migration during *Drosophila* development

At an organismal level, RN-tre is associated with aberrant cell migration during the development of the *Drosophila* nervous system and oogenesis. Misexpression of RN-tre in mushroom bodies leads to axonal growth and guidance defects (Nicolaï *et al.*, 2003). Similarly, the misexpression of RN-tre in photoreceptor cells (R-cells) led to a loss in apical positioning (Houalla *et al.*, 2010). In the case of R-cell positioning, RN-tre displayed a dosage-dependent interaction with Rabs 5 and 11 and thus the phenotype is at least partially dependent on RN-tre's GAP activity. It was assumed that RN-tre was also acting as a GAP during mushroom body development however, given RN-tre's ability to interact with the cytoskeleton, further research is needed to clearly define its role during this process. While these two studies examined the overexpression of RN-tre during development of the nervous system, depletion of RN-tre in border cells inhibited their migration (Laflamme *et al.*, 2012). Here again, Laflamme and colleagues suggest that RN-tre is acting as a GAP for Rab5 in this capacity. However, expression of a dominant negative Rab5 also inhibited border cell migration, suggesting that both an overactive and underactive Rab5 can inhibit this process (Assaker *et al.*, 2010). While border cell migration may be sensitive to the precise dosage of Rab5, the possibility exists that RN-tre is also

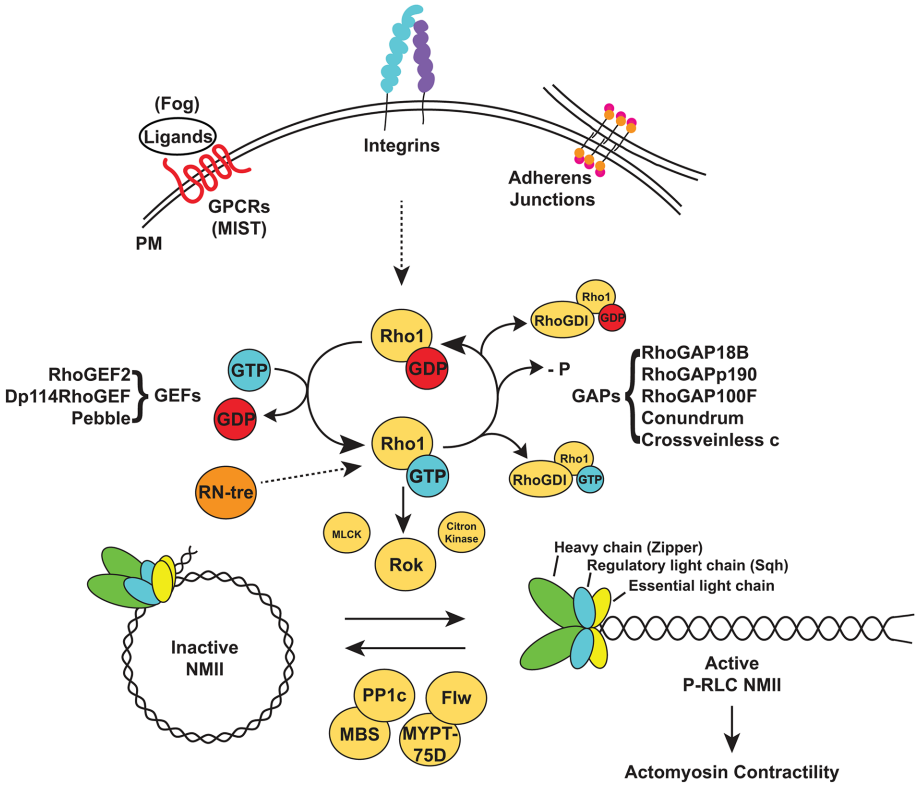

FIGURE 9: Model of Rho1 activation. Various signals including ligand–GPCR interactions, integrin, and adherens junction signaling converge on Rho1 signaling (Chountala *et al.*, 2012; Manning *et al.*, 2013; LeBlanc and Lehmann, 2017; Silver *et al.*, 2019). RN-tre is a known Rab GTPase-activating protein (GAP) that was shown herein to regulate Rho1 signaling by regulating the amount of active Rho1 in *Drosophila* S2 cells. Inactive GDP-bound Rho1 is activated by a multitude of guanine nucleotide exchange factors (GEFs), including RhoGEF2, Dp114RhoGEF, and Pebble (Aguilar-Aragon *et al.*, 2020), that exchange GDP for GTP. Rho1-GTP can activate Rho kinase (Rok), which phosphorylates regulatory light chain (RLC, encoded by the *Drosophila* gene *spaghetti squash* or *sqh*) of nonmuscle myosin II (NMII). Myosin light chain kinase (MLCK) and citron kinase are additional minor contributors to NMII activation. When the RLC is phosphorylated on an inactive autoinhibited NMII hexamer, NMII becomes uninhibited and takes a conformation more favorable to binding actin and making higher-order oligomers. More active NMII contributes to increased actomyosin contractility. The myosin phosphatase-targeting subunit MYPT-75D targets Flapwing (Flw; PP1β9C) to NMII where Flw dephosphorylates the RLC, and it is postulated that PP1c has dephosphorylation activity for RLC as well, it being trafficked by the myosin phosphatase-targeting subunit myosin-binding subunit (MBS) (Kirchner *et al.*, 2007). Various Rho GAPs (including RhoGAP18B, RhoGAPp190, RhoGAP100F, Conundrum, and Crossveinless c) inactivate Rho1 by facilitating the dephosphorylation of GTP bound to Rho1 (Billuart *et al.*, 2001; Denholm *et al.*, 2005; Neisch *et al.*, 2013; Ojelade *et al.*, 2015; Spinner *et al.*, 2018). Rho guanine nucleotide dissociation inhibitor (GDI) dampens Rho1 signaling by sequestering both active and inactive Rho1 (Guruharsha *et al.*, 2011; Oishi *et al.*, 2012).

affecting migration through the cytoskeleton and, more specifically as we have shown here, through NMII. Not surprisingly, depletion of NMII and other proteins in the Rho1 pathway also leads to defects in border cell migration (Combedazou *et al.*, 2017)

Conclusion

The results presented here point to a role for the Rab GAP RN-tre in regulating NMII contractility. We show that RN-tre depletion leads to a subsequent decrease in Rho1 signaling, ultimately leading to less phosphorylated RLC. Furthermore, we found that RN-tre's GAP activity was only partially required for this role. These results are yet another example of cross-talk between a cell's transport machinery and the cytoskeleton and may have further implications in processes such as cell migration and morphogenesis.

MATERIALS AND METHODS

Plasmid construction

To construct RNAi-resistant *rn-tre* constructs, an *rn-tre* gene fragment that spans the RN-Tre3 RNAi targeting sequence (nucleotides 1266–1601) was designed in silico to have 112 silent mutations of 337 nucleotides (67% identical) and ordered from Twist Biosciences (San Francisco, CA). A coisogenic fragment with a R153A substitution was ordered. The two gene fragments and a pMT/V5-HisA-derivative with *rn-tre* and a Myc-tag at the C-terminus were amplified by Q5 Hot Start High-Fidelity DNA Polymerase (New England Biolabs, Ipswich, MA) and cloning primers (see Table 1 later in this article) by the manufacturer's instructions. The vector and inserts were gel purified with the Zymoclean Gel DNA Recovery Kit by following the manufacturer's instruction (Zymo Research, Irvine, CA). Gibson Assembly (NEB) reactions of 113 ng vector and 20 ng insert (~3:1 molar ratio of inserts to vector) were incubated at 50°C for 15 min and then on ice for 20 min. Assemblies were transformed into the NEB 5-alpha competent *Escherichia coli* (High Efficiency) and selected. Cloned regions were confirmed to be correct without error by sequencing (ACGT, Wheeling, IL) and confirmed to be in-frame by expression in S2R+ cells and immunostaining against Myc, as well as by Western blot against Myc.

Cell culturing

For a detailed description of *Drosophila* cell culturing, see Rogers and Rogers (2005) and Applewhite *et al.* (2014). Cells were cultured in Shields and Sang media (S&S; Sigma S8398, 0.5 g/l $NaHCO_3$, 1 g/l yeast extract, 2.5 g/l bactopeptone) with 10% fetal bovine serum (FBS) (Thermo Fisher Scientific, Waltham, MA) and 1× Antibiotic-Antimycotic (Life Technologies; 15240-062) at 25°C (Tables 2 and 3).

RNAi treatment

For detailed instructions on how to obtain dsRNA suitable for insect culture, see Rogers and Rogers (2005). Cells were incubated with 1 µl of dsRNA in 1 ml of S&S media in six-well plates at 25°C for 24 h (Table 4). Media and dsRNA were aspirated off and replenished each day of treatment, typically 5–7 d.

Transfections

Transfections were carried out using the FuGENE HD Transfection Reagent (Promega, Madison, WI) following the manufacturer's instructions. Briefly, FuGENE Reagent was brought to room temperature. Plasmid DNA (2 g) was added to up to 100 µl of water. FuGENE Reagent (6 µl) was added to DNA and mixed by pipetting immediately. The mixture was incubated at room temperature for 10 min.

Name	Sequence (5′ to 3′)[a]
RNtreRNAiResistVector_fwd	atcagaagtatggaatgcACGGGCTGTTTATCGAGG
RNtreRNAiResistVector_rev	ccaacaatttgttccaggCCACCATACGCACGCGATC
RNtreRNAiResistInsert_fwd	CCTGGAACAAATTGTTGG
RNtreRNAiResistInsert_rev	GCATTCCATACTTCTGATC

[a]Lowercase letters prime to the vector, uppercase letters prime to the insertion sequence.

TABLE 1: Cloning primers.

Cell line	Expression	Selection	Source
S2			DGRC[a]
S2R+			DGRC
ML-Dm25-c2 (D25)			DGRC
S2R+: pSqh::Sqh-EGFP/pCoHygro	Sqh-EGFP	Hygromycin B	DGRC
S2: pMTFog-Myc/pCoHygro	Copper-inducible Fog-Myc	Hygromycin B	—[b]
S2R+: pMTRN-treWTRRMyc/pCoHygro		Hygromycin B	this study
S2R+: pMTRN-treR153ARRMyc/pCoHygro		Hygromycin B	this study

[a]DGRC, Drosophila Genomics Resource Center, Bloomington, IN.
[b]Manning *et al.*, 2013; Peters and Rogers, 2013; Peters *et al.*, 2018.

TABLE 2: *Drosophila melanogaster* cell lines.

Name	Genetics	Selection	Source
pMTFogMyc	Fog-Myc		DGRC[a]
pMT RN-treWTRRMyc	RNAi resistant		
pMT RN-treR153ARRMyc	RNAi resistant with R153A substitution		
pMT SQH::SQH-EGFP	Sqh-EGFP		Rogers *et al.*, 2004
pCoHygro		Hygromycin B	Invitrogen
pMT/GFP/Blast	Soluble GFP	Blasticidin S	Invitrogen

[a]DGRC, Drosophila Genomics Resource Center, Bloomington, IN.

TABLE 3: Plasmids.[a]

The DNA–water mixture was then added dropwise to cells that were ~80–100% confluent in 1 ml media six-well plate. $CuSO_4$ (1 mM) was added to cells if necessary for induction of pMT constructs.

Coalescence index

S2R+: SQH-EGFP or S2R+ cells were treated with appropriate dsRNA as described above for 7 d, with transient transfection as needed. Cells were then plated on convacalin A (ConA)-coated coverslips and live-imaged on a Nikon Eclipse Ti-E inverted microscope (Nikon, Tokyo, Japan) using a 100×/1.49NA oil immersion TIRF objective driven by Nikon Elements software. Images were captured using an Orca-Flash 4.0 (Hamamatsu, Japan). EGFP localization was quantified in ImageJ (version 2.0.0-rc-69/1.52i). The coalescence index was quantified by modifying the analysis performed in Bouchier-Hayes *et al.* (2008). Briefly, images of cells were thresholded in ImageJ and the cell was outlined. All values for the *XY* coordinates surrounded by the outline were obtained and normalized to a scale of 0–1. The mean over the SD of the normalized values was designated the "coalescence index" and compared across conditions. High values indicate more fluorescent pixel coalescence, while low values indicate dispersed fluorescent pixels.

Phosphomyosin staining

Cells were treated with appropriate dsRNA for 7 dand then plated on ConA-coated coverslips for 30–40 min and fixed in 10% paraformaldehyde (Electron Microscopy Sciences, Hatfield, PA) in PEM buffer (100 mM PIPES-sodium salt, 1 mM ethylene glycol-bis(β-aminoethyl ether)-*N*,*N*,*N*′,*N*′-tetraacetic acid, 1 mM $MgCl_2$) at room temperature for 15 min. Cells were washed 3× in phosphate-buffered saline (PBS) or Tris-buffered saline (TBS; 20 mM Tris, 150 mM NaCl, pH 7.4), blocked in 5% normal goat serum in PBS with 0.1% Triton-X for 20 min, incubated with 1:200 rabbit anti-phosphomyosin light chain 2 (Ser-19) antibody (Cell Signaling Technology, Danvers, MA), and then washed 3× in PBS or TBS and incubated with 1:100 AlexaFluor-488 or -594–conjugated anti-rabbit secondary antibody, with 1:100 phalloidin, and Hoechst for 1 h. Cells were washed 3× in PBS and covered in mounting media (Dako anti-fade mounting media; Agilent, Santa Clara, CA). Cells were imaged by TIRF and tallied as "phospho-myosin-positive" if the staining was clear or "-negative" if it was not. This was expressed as a fraction, with the number of phosphomyosin-positive cells over the total number of cells counted.

dsRNA	CG #	Forward (5′ to 3′)[a]	Reverse (5′ to 3′)[a]	Reference
Alpha-Actinin	CG4376	AGGATTCGGAAGGAGTCGAT	GGTGCAGGAATCGATGATCT	Flockhart *et al.*, 2006
Control		GGCAGGGGTTGGGGTATT	GCGCAGAAGAACAAAAAGAA	Rogers and Rogers, 2008
Dia	CG1768	AAGTAGGGCTCGGAAGTGGT	CTGCATTGTCTATGAGCGGA	Rogers *et al.*, 2003
Mlc-c	CG3201	CCGATTCTAGCTGTTCAACTGTCC	GTGTCAATTTTAGAATAATACGC	
Rab5	CG3664	GCAGTAACCGTCCGTAGAACC	GTCCCAGATCTCGAACTTAACG	Rogers *et al.*, 2003
Rab6	CG6601	GTCTGGTGGAACGAGTTGGT	GACGGAAAGCATTTAGAGCG	Flockhart *et al.*, 2006
Rab19	CG7062	GCGAGGTGGACTTTGAAGAG	TGACATTGTTGGCTCGATTC	Flockhart *et al.*, 2006
Rho1	CG8416	ATCAAGAACAACCAGAACATCG	TTTGTTTTGTGTTTAGTTCGGC	Rogers *et al.*, 2003
RhoGEF2	CG9635	ATGGATCACCCATCAATCAAAAAAC-GG	TGTCCCGATCCCTATGACCACTA-AGGC	Rogers *et al.*, 2004
RN-tre	CG8085	ACTTAATAGCGTACAGCAGGGC	GGATGAAGATGCTAAATCAGTGG	Stephen L. Rogers
RN-tre2	CG8085	TTCCACGAAGACGACAAAG	ATCGCGTGCGTATGGTG	Flockhart *et al.*, 2006
RN-tre3	CG8085	GCATGCCGTATTTTTGGTCT	CCTGGAATAAGCTGCTCGAC	Flockhart *et al.*, 2006
Rok1	CG9774	GAGAACACTCAAAAGCTGAAAAAG	ACAGTTCCTTCTGTAGCTGGTTTT	Rogers *et al.*, 2003
Sqh	CG3595	GCCCGGGATCAACTTCATGTTCCTC	TGTCCTTGGCACCGTGCTTAAGG	Rogers *et al.*, 2003
Ssh	CG6238	GGAGATCGATAACTTCTTTCCG	GTTCTCCATAGACTGGCTTTGC	Rogers *et al.*, 2003
Zipper	CG15792	CCTAAAGCCACTGACAAGACG	CGGTACAAGTTCGAGTCAAGC	Rogers *et al.*, 2003

[a]All primers have the T7 promoter sequence (taatacgactcactatagg) on the 5′ end.

TABLE 4: T7 primers.

Kymography

Kymograph analyses were based on methods described in Iwasa and Mullins (2007) and were analyzed using ImageJ. Briefly, 4-μm-thick lines were used to generate kymographs, and individual tracks were traced by hand. Three to six kymographs were produced for each cell, and 15–30 cells were analyzed per RNAi condition. The slope of the individual tracks was calculated and used to find rates.

Fog harvesting

For a detailed description of Fog media harvesting, see Peters *et al.* (2018). $CuSO_4$ (1 mM) was added to S2: pMTFog-Myc cells were grown to 100% confluency and incubated at 25°C for 48–72 h. Cells were pelleted at 2734 × *g* for 10 min at 4°C. The supernatant was concentrated by transfer to a 3K NMWL Ultra-4 centrifugal filter (Merck Millipore, Tullagreen, Ireland) and centrifuged at up to 7500 × *g* for 1–2 h increments at 4°C, collecting the darker brown fractions each time. Fog was confirmed by Western blot using a mouse anti-Myc 9E10-S 1° antibody (Developmental Hybridoma Bank, Iowa City, IA) and an anti-mouse immunoglobulin G (IgG) horseradish peroxidase (HRP)-linked 2° antibody (Cell Signaling Technology, Danvers, MA) and developed by SuperSignal West PICO Plus Chemiluminescent Substrate (Thermo Scientific). Concentrated Fog media was stored at 4°C for up to 3 mo.

Cell constriction assay

For a detailed description of the assay protocol, see Peters *et al.* (2018). Cells were treated with appropriate dsRNA for 7 d and induced with 1 mM $CuSO_4$ on day 5 where appropriate. Cells (~100 μl) were added to 2 ml S&S media on ConA-coated coverslips and left to attach for 40 min. Excess media was aspirated off, 150 μl of fresh S&S media was pipetted on, and 50 μl of Fog or control media was added to the coverslips. After 8 min, media was aspirated off and an excess of fresh 10% paraformaldehyde solution in PEM buffer was added and cells were left to fix at room temperature for 15 min. The paraformaldehyde solution was aspirated off, and the cells were gently washed three times in PBS. Coverslips were incubated with 1:100 Alexa-564 Phalloidin (Thermo Fisher Scientific, Waltham, MA) and 1× Hoechst 33258 (Thermo Fisher Scientific) in PBS + 0.1% Triton X-100 (Sigma) at room temperature for 30 min. Coverslips were gently rinsed three times in PBS. Dako fluorescence mounting medium was added to the coverslips, and cells were imaged at 40× by phase-contrast microscopy on a Nikon Eclipse Ti-E inverted microscope. Two hundred cells were counted per condition and noted for contractility.

Active Rho pull down

The amount of active Rho1 was determined using the Rho Activation Assay Biochem Kit (Cytoskeleton, Denver, CO) by following the manufacturer's instructions. Two six-well plates of cells were treated with appropriate dsRNA—RN-tre, control, or untreated–as described above for 7 d. On day 5, cells were serum starved by replacing media with S&S media with 1% FBS, and on day 6, media was replaced with S&S media without FBS. Cells were put on ice, and the media was aspirated off. Cells were gently washed with 10 ml ice-cold sterile-filtered PBS, and the PBS was aspirated off. Cells were allowed to sit on a slight incline on ice for 1 min, and residual PBS was pipetted off. Cells were resuspended in 1 ml of kit lysis buffer per condition and centrifuged at 17,000 × *g* at 4°C for 10 min, and the supernatant was removed to a new tube. Lysates were snap-frozen on dry ice/ethanol. The protein concentration from each sample was quantified by diluting 1/10th in lysis buffer and using the Protein Assay Dye Reagent Micro Assay (Bio-Rad, Hercules, CA). Samples were unfrozen on room temperature water and diluted to 1.2 mg/ml total protein in lysis buffer. A total of 600 μg (500 μl) of total protein was incubated with 15 μl of Rhotekin-RBD beads. Samples were incubated at 4°C with rocking for 1 h. Samples were centrifuged at 2500 × *g* at 4°C for 1 min. Ninety percent of the supernatant was carefully removed. Beads

were washed once by adding 500 µl kit wash buffer and centrifuged at 2500 × *g* at 4°C for 3 min. The supernatant was carefully removed, and beads were resuspended in 20 µl 2× Laemmli sample buffer (BioRad) with 5% β-mercaptoethanol. Samples (10 µl) were run on precast 10% Mini-Protean TGX gels (BioRad), transferred to nitrocellulose (BioRad), and blotted with 1:200 mouse anti-Rho1 1° antibody (Developmental Hybridoma Bank) or 1:500 mouse anti–β-tubulin 1° antibody (Developmental Hybridoma Bank) in Tris-buffer saline plus 0.1 Triton X-100 (TBST) with 5% milk at 4°C overnight. The blot was washed three times in 10 ml TBST at room temperature with rocking and then incubated in 1:5000 anti-mouse IgG HRP-conjugated 2° antibody (Cell Signaling Technology, Danvers, MA) in TBST with 5% milk, rocking at room temperature. The blot was washed three times as before and developed by SuperSignal Chemiluminescent Substrate.

RT-qPCR

Experimental design and samples. Two dishes of roughly 1.2 × 10^6 *D. melanogaster* S2R+ cells were treated with corresponding dsRNAi for 7 d (as described). Adherent cells were washed from the well bottom by pipette and pipetted into microfuge tubes. The cells were pelleted at 300 × *g* for 3 min, and the media was decanted. Cells were kept on ice and immediately processed for RNA extraction.

Nucleic acid extraction. Total RNA from freshly lysed cells was extracted by the Maxwell 16 Low Elution Volume simplyRNA Cells Kit in a Maxwell 16 (Promega, Madison, WI). Maxwell kit supplies were used for all subsequent steps of extraction. Cold 1-thioglycerol (4 µl) in 200 µl homogenization solution was added to the cell pellet, and the pellet was vortexed for 10 s until it was dispersed. Cold lysis buffer (200 µl) from the Maxwell kit (Part# MC501C) was added to cells and vortexed vigorously for 15 s. Whole lysate mixture (400 µl) was pipetted into the Maxwell 16 LEV Cartridge (MCE) along with DNase I solution (5 µl). Maxwell was run with LEV settings as per the manufacturer's instructions. Upon completion, samples were immediately removed and snap frozen on a dry ice/ethanol mixture. Samples were stored at –80°C for up to 24 h prior to reverse transcription while quantified.

RNA quantification and quality assessment. Total RNA was subjected to NanoDrop 1000 (Thermo Fisher Scientific) analysis (Supplemental Table 1). RNA integrity was visualized on a 1% wt/vol agarose with 1% vol/vol bleach gel in Tris-acetate-EDTA buffer (TAE) at 60 V at 4°C for more than an hour (Aranda *et al.*, 2012). In visualization, the bands were qualitatively determined to have intensity ratios of the 28S/18S bands 1–2, no visible smear below 18S, and no material stuck in the well, which can be an indication of genomic DNA contamination. Further DNA contamination controls were performed in the qPCR amplification step.

Reverse transcription. Reverse transcription was carried out with the Promega GoScript Reverse Transcription System (#A5000; Promege, Madison, WI) according to the manufacturer's instructions. Here, in duplicate per RNAi reaction, 3.25 µg of RNA was added to 0.5 µg of Oligo$(dT)_{15}$ primer in nuclease-free water up to 5 µl. The RNA primer mix was incubated at 70°C for 5 min, chilled on ice water for 5 min, and then spun down for 5 s. A reverse transcription master mix was prepared by mixing together (per reaction) 7.2 µl nuclease-free water, 4 µl GoScript 5X Reaction Buffer, 1.2 µl $MgCl_2$ (1.5 mM final), 1 µl PCR nucleotide mix (0.5 mM each final), 20 U recombinant RNasin ribonuclease inhibitor, and 1 µl GoScript Reverse Transcriptase. Aliquots of 15 µl were added to the 5 µl RNA/Oligo$(dT)_{15}$ mix. A no-reverse transcriptase control for each condition was included. Reactions were incubated at 25°C for 5 min, 42°C for 1 h, and then 70°C for 15 min. Reactions were aliquoted into 4-µl portions, snap-frozen on dry ice/70% ethanol, and stored at –80°C. cDNA was not subjected to more than one freeze-thaw prior to use for qPCR.

qPCR targets and oligonucleotides. RT-qPCR primers were ordered from QIAGEN (Hilden, Germany): RN-tre (Dm_RN-tre_1_SG, QT00946393) and reference gene EF1 (Dm_Ef1alpha100E_2_SG, QT00511574). Relevant primer information from QIAGEN is given in Table 5.

qPCR protocol. The Promega GoTaq qPCR Master Mix (A6001) was used for reactions. The mix has a proprietary dsDNA-binding dye that is detected by SYBR Green I filters and settings. The Taq polymerase and buffer composition is proprietary. Reactions of 20 µl were composed of 4 µl nuclease-free water, 10 µl GoTaq MasterMix (1× final), 2 µl primers (1× final), and 4 µl template cDNA. cDNA was diluted 10-fold and then used for quantification runs. For every run, a master PCR mix was manually made in a BioExpress AirClean 600 PCR Workstation hood and aliquoted into opaque, 96-well PCR plates (BioRad; MLL9651), and then template was added separately. Plates were sealed by Microseal "B" film (BioRad; MSB1001) and spun down. qPCR was performed in a CFX Connect Real Time System (BioRad). Thermal cycling parameters were as follows: incubation at 1) 95°C for 2 min, 2) 95°C for 15 s, 3) 55°C for 40 s, 4) 72°C for 30 s, and take acquisition, 5) go to step 2 44 more times, 6) 65–97°C at 0.5°C increments every 5 s.

qPCR validation. Standard curves of cDNA dilutions were run for both primer sets to determine efficiency. From an eight-point,

Target	Name	Catalogue no.	Transcript variants	NCBI Accession No.	Amplicon length (base pairs)	Location (# exons)
RN-tre	Dm_RN-tre_1_SG	QT00946393	A	NM_144124	107	5′ UTR[a] (1/2)
			C	NM_166028	107	5′ UTR (1/2)
EF1	Dm_Ef1alpha100E_2_SG	QT00511574	A	NM_079872	84	5′ UTR (2/3)
			B	NM_170570	84	5′ UTR (2/3)
			D	NM_206592	81	5′ UTR (2/3)
			C	NM_206593	81	5′ UTR (2/3)

[a]UTR, untranslated region.

TABLE 5: RT-qPCR QIAGEN primer pairs.

10-fold dilution curve in triplicate, RN-tre primers were found to be 102.0% efficient (slope = –3.276, *y*-int. = 18.955, R^2 = 0.993). RN-tre products melted at 77.0–77.5°C. None of the "no template" controls or the "no reverse transcriptase" controls fired in 45 cycles. Dilutions below 10^{-5} had some technical replicates that did not fire. Thus, the linear dynamic range for this primer set was 10^{-1}–10^{-5}, or 16.25–1.625 × 10^{-3} ng/µl total cDNA concentration, assuming a 1:1 reverse transcription reaction. The quantification cycle (Cq) SD at the lower limit was 0.717. From an eight-point 10-fold dilution curve in triplicate, SK primers were found to be 107.7% efficient (slope = –3.150, *y*-int. = 22.701, R^2 = 0.991). SK products melted at 77.5–78.0°C. Single reactions from dilutions were run out on a gel to verify single product bands. None of the "no template" controls or the "no reverse transcriptase" controls fired in 45 cycles. Dilutions below 10^{-4} had some technical replicates that did not fire. Thus, the linear dynamic range for the assay was 10^{-1}–10^{-4} cDNA, or 16.25–1.625 × 10^{-2} ng/µl total cDNA concentration, assuming a 1:1 reverse transcription. The Cq SD at the lower limit was 0.769. Five-point, fivefold dilution curves starting with a 1× cDNA were run in triplicate for both of the primers and were similarly efficient to the 10-fold dilution curves. Single runs from these curves were run on a gel to verify single-band products of appropriate size. PCR efficiency was not inhibited up to 1× cDNA amplification.

Data analysis

Real-time data were collected and analyzed in Bio-Rad CFX Manager 3.1 software by the ΔΔCq method. The Cq single threshold was autocalculated. Any Cq ≥ 38 was excluded from analysis. None of the no-template controls fired in 38 cycles for either primer pair in any run. EF1 was chosen as a reference gene because it, along with tubulin, was found to be most stable in *Drosophila* in a study of seven candidate reference genes (Ponton *et al*., 2011).

ACKNOWLEDGMENTS

We acknowledge the Drosophila Genomics Resources Center (DGRC) (National Institutes of Health [NIH] grant 2P40OD010949 to DGRC) and the Developmental Studies Hybridoma Bank created by the Eunice Kennedy Shriver National Institute of Child Health and Human Development of the NIH and maintained at the Department of Biology, The University of Iowa, Iowa City, for reagents. Members of the Applewhite lab, Rogers lab, Peifer lab (University of North Carolina, Chapel Hill), and Slep lab (University of North Carolina, Chapel Hill) for their thoughtful discussions during the preparation of this article. Additionally, we thank Greta Glover and Kristine Hayes for their support with equipment and reagents. This work was supported by the National Science Foundation (NSF 716964 to D.A.A. and A.R.) and the Reed College Department of Biology.

REFERENCES

Abreu-Blanco MT, Verboon JM, Parkhurst SM (2014). Coordination of Rho family GTPase activities to orchestrate cytoskeleton responses during cell wound repair. Curr Biol 24, 144–155.

Afshar K, Stuart B, Wasserman SA (2000). Functional analysis of the Drosophila diaphanous FH protein in early embryonic development. Development 127, 1887–1897.

Aguilar-Aragon M, Bonello TT, Bell GP, Fletcher GC, Thompson BJ (2020). Adherens junction remodelling during mitotic rounding of pseudostratified epithelial cells. EMBO Rep 21, 690–703.

Aguilar-Cuenca R, Juanes-García A, Vicente-Manzanares M (2014). Myosin II in mechanotransduction: master and commander of cell migration, morphogenesis, and cancer. Cell Mol Life Sci 71, 479–492.

Amano M, Ito M, Kimura K, Fukata Y, Chihara K, Nakano T, Matsuura Y, Kaibuchi K (1996). Phosphorylation and activation of myosin by Rho-associated kinase (Rho-kinase). J Biol Chem 271, 20246–20249.

Applewhite DA, Davis CA, Griffis E R, Quintero OA (2014). Imaging of the cytoskeleton using live and fixed Drosophila tissue culture cells. Methods Mol Biol 1365, 83–97.

Aranda PS, LaJoie DM, Jorcyk CL (2012). Bleach gel: a simple agarose gel for analyzing RNA quality. Electrophoresis 33, 366–369.

Assaker G, Ramel D, Wculek SK, González-Gaitán M, Emery G (2010). Spatial restriction of receptor tyrosine kinase activity through a polarized endocytic cycle controls border cell migration. Proc Natl Acad Sci USA 107, 22558–22563.

Barrett K, Leptin M, Settleman J (1997). The Rho GTPase and a putative RhoGEF mediate a signaling pathway for the cell shape changes in Drosophila gastrulation. Cell 91, 905–915.

Barylko B, Tooth P, Kendrick-Jones J (1986). Proteolytic fragmentation of brain myosin and localisation of the heavy-chain phosphorylation site. Eur J Biochem 158, 271–282.

Bielli A, Thörnqvist PO, Hendrick AG, Finn R, Fitzgerald K, McCaffrey MW (2001). The small GTPase Rab4A interacts with the central region of cytoplasmic dynein light intermediate chain-1. Biochem Biophys Res Commun 281, 1141–1153.

Billuart P, Winter CG, Maresh A, Zhao X, Luo L (2001). Regulating axon branch stability: the role of p190 RhoGAP in repressing a retraction signaling pathway. Cell 107, 195–207.

Borg M, Bakke O, Progida C (2014). A novel interaction between Rab7b and actomyosin reveals a dual role in intracellular transport and cell migration. J Cell Sci 127, 4927–4939.

Bouchier-Hayes L, Muñoz-Pinedo C, Connell S, Green DR (2008). Measuring apoptosis at the single cell level. Methods 44, 222–228.

Cai Y, Biais N, Giannone G, Tanase M, Jiang G, Hofman JM, Wiggins CH, Silberzan P, Buguin A, Ladoux B, *et al.* (2006). Nonmuscle myosin IIA-dependent force inhibits cell spreading and drives F-actin flow. Biophys J 91, 3907–3920.

Cantalupo G, Alifano P, Roberti V, Bruni CB, Bucci C (2001). Rab-interacting lysosomal protein (RILP): the Rab7 effector required for transport to lysosomes. EMBO J 20, 683–693.

Chen PW, Jian X, Heissler SM, Le K, Luo R, Jenkins LM, Nagy A, Moss J, Sellers JR, Randazzo PA (2016). The Arf GTPase-activating protein, ASAP1, binds nonmuscle myosin 2A to control remodeling of the acto-myosin network. J Biol Chem 291, 7517–7526.

Chountala M, Vakaloglou KM, Zervas CG (2012). Parvin overexpression uncovers tissue-specific genetic pathways and disrupts F-actin to induce apoptosis in the developing epithelia in Drosophila. PLoS One 7, e47355.

Christoforidis S, Miaczynska M, Ashman K, Wilm M, Zhao L, Yip SC, Waterfield MD, Backer JM, Zerial M (1999). Phosphatidylinositol-3-OH kinases are Rab5 effectors. Nat Cell Biol 1, 249–252.

Chrzanowska-Wodnicka M, Burridge K (1996). Rho-stimulated contractility drives the formation of stress fibers and focal adhesions. J Cell Biol 133, 1403–1415.

Collins JH, Côté GP, Korn ED (1982a). Localization of the three phosphorylation sites on each heavy chain of Acanthamoeba myosin II to a segment at the end of the tail. J Biol Chem 257, 4529–4534.

Collins JH, Kuznicki J, Bowers B, Korn ED (1982b). Comparison of the actin binding and filament formation properties of phosphorylated and dephosphorylated Acanthamoeba myosin II. Biochemistry 21, 6910–6915.

Combedazou A, Choesmel-Cadamuro V, Gay G, Liu J, Dupré L, Ramel D, Wang X (2017). Myosin II governs collective cell migration behaviour downstream of guidance receptor signalling. J Cell Sci 130, 97–103.

Costa M, Wilson ET, Wieschaus E (1994). A putative cell signal encoded by the folded gastrulation gene coordinates cell shape changes during Drosophila gastrulation. Cell 76, 1075–1089.

Côté GP, Robinson EA, Appella E, Korn ED (1984). Amino acid sequence of a segment of the Acanthamoeba myosin II heavy chain containing all three regulatory phosphorylation sites. J Biol Chem 259, 12781–12787.

Cotton M, Boulay PL, Houndolo T, Vitale N, Pitcher JA, Claing A (2007). Endogenous ARF6 interacts with Rac1 upon angiotensin II stimulation to regulate membrane ruffling and cell migration. Mol Biol Cell 18, 501–511.

Cramer LP (2000). Myosin VI: roles for a minus end-directed actin motor in cells. J Cell Biol 150, F121–F126.

Dawes-Hoang RE, Parmar KM, Christiansen AE, Phelps CB, Brand AH, Wieschaus EF (2005). folded gastrulation, cell shape change and the control of myosin localization. Development 132, 4165–4178.

Dean SO, Spudich JA (2006). Rho kinase's role in myosin recruitment to the equatorial cortex of mitotic Drosophila S2 cells is for myosin regulatory light chain phosphorylation. PLoS One 1, e131.

Dechamps C, Bach S, Portetelle D, Vandenbol M (2006). The Tre2 oncoprotein, implicated in Ewing's sarcoma, interacts with two components of the cytoskeleton. Biotechnol Lett 28, 223–231.
de las Bayonas AG, Philippe JM, Lellouch AC, Lecuit T (2019). Distinct RhoGEFs activate apical and junctional 1 actomyosin contractility under control of G proteins during epithelial morphogenesis. SSRN Electronic J, DOI: 10.2139/ssrn.3363748.
Denholm B, Brown S, Ray RP, Ruiz-Gómez M, Skaer H, Hombría JCG (2005). crossveinless-c is a RhoGAP required for actin reorganisation during morphogenesis. Development 132, 2389–2400.
Dorsten JN, Kolodziej PA, VanBerkum MFA (2007). Frazzled regulation of myosin II activity in the Drosophila embryonic CNS. Dev Biol 308, 120–132.
Dulyaninova NG, Bresnick AR (2013). The heavy chain has its day: regulation of myosin-II assembly. BioArchitecture 3, 77–85.
Echard A, Jollivet F, Martinez O, Lacapère JJ, Rousselet A, Janoueix-Lerosey I, Goud B (1998). Interaction of a Golgi-associated kinesin-like protein with Rab6. Science 279, 580–585.
Encarnação M, Espada L, Escrevente C, Mateus D, Ramalho J, Michelet X, Santarino I, Hsu VW, Brenner MB, Barral DC, *et al*. (2016). A Rab3a-dependent complex essential for lysosome positioning and plasma membrane repair. J Cell Biol 213, 631–640.
Even-Ram S, Doyle AD, Conti MA, Matsumoto K, Adelstein RS, Yamada KM (2007). Myosin IIA regulates cell motility and actomyosin-microtubule crosstalk. Nat Cell Biol 9, 299–309.
Flockhart I, Booker M, Kiger A, Boutros M, Armknecht S, Ramadan N, Richardson K, Xu A, Perrimon N, Mathey-Prevot B (2006). FlyRNAi: the Drosophila RNAi screening center database. Nucleic Acids Res 34, D489–D494.
Fox DT, Peifer M (2007). Abelson kinase (Abl) and RhoGEF2 regulate actin organization during cell constriction in Drosophila. Development 134, 567–578.
Frasa MAM, Koessmeier KT, Ahmadian MR, Braga VMM (2012). Illuminating the functional and structural repertoire of human TBC/RABGAPs. Nat Rev Mol Cell Biol 13, 67–73.
Gertler FB, Comer AR, Juang JL, Ahern SM, Clark MJ, Liebl EC, Hoffmann FM (1995). enabled, a dosage-sensitive suppressor of mutations in the Drosophila Abl tyrosine kinase, encodes an Abl substrate with SH3 domain-binding properties. Genes Dev 9, 521–533.
Guruharsha KG, Rual JF, Zhai B, Mintseris J, Vaidya P, Vaidya N, Beekman C, Wong C, Rhee DY, Cenaj O, *et al*. (2011). A protein complex network of Drosophila melanogaster. Cell 147, 690–703
Haas AK, Fuchs E, Kopajtich R, Barr FA (2005). A GTPase-activating protein controls Rab5 function in endocytic trafficking. Nat Cell Biol 7, 887–893.
Haas AK, Yoshimura S, Stephens DJ, Preisinger C, Fuchs E, Barr FA (2007). Analysis of GTPase-activating proteins: Rab1 and Rab43 are key Rabs required to maintain a functional Golgi complex in human cells. J Cell Sci 120, 2997–3010.
Hales CM, Vaerman JP, Goldenring JR (2002). Rab11 family interacting protein 2 associates with myosin Vb and regulates plasma membrane recycling. J Biol Chem 277, 50415–50421.
Hammer JA, Sellers JR (2011). Walking to work: roles for class V myosins as cargo transporters. Nat Rev Mol Cell Biol 13, 13–26.
Heissler SM, Sellers JR (2016). Various themes of myosin regulation. J Mol Biol 428, 1927–1946.
Higgs HN, Pollard TD (2000). Activation by Cdc42 and PIP(2) of Wiskott-Aldrich syndrome protein (WASp) stimulates actin nucleation by Arp2/3 complex. J Cell Biol 150, 1311–1320.
Hoepfner S, Severin F, Cabezas A, Habermann B, Runge A, Gillooly D, Stenmark H, Zerial M (2005). Modulation of receptor recycling and degradation by the endosomal kinesin KIF16B. Cell 121, 437–450.
Homem CCF, Peifer M (2008). Diaphanous regulates myosin and adherens junctions to control cell contractility and protrusive behavior during morphogenesis. Development 135, 1005–1018.
Honda A, Nogami M, Yokozeki T, Yamazaki M, Nakamura H, Watanabe H, Kawamoto K, Nakayama K, Morris AJ, Frohman MA, *et al*. (1999). Phosphatidylinositol 4-phosphate 5-kinase alpha is a downstream effector of the small G protein ARF6 in membrane ruffle formation. Cell 99, 521–532.
Houalla T, Shi L, van Meyel DJ, Rao Y (2010). Rab-mediated vesicular transport is required for neuronal positioning in the developing Drosophila visual system. Mol Brain 3, 19.
Huang J, Imamura T, Olefsky JM (2001). Insulin can regulate GLUT4 internalization by signaling to Rab5 and the motor protein dynein. Proc Natl Acad Sci USA 98, 13084–13089.
Imamura T, Huang J, Usui I, Satoh H, Bever J, Olefsky JM (2003). Insulin-induced GLUT4 translocation involves protein kinase C-lambda-mediated functional coupling between Rab4 and the motor protein kinesin. Mol Cell Biol 23, 4892–4900.
Ishibashi K, Kanno E, Itoh T, Fukuda M (2009). Identification and characterization of a novel Tre-2/Bub2/Cdc16 (TBC) protein that possesses Rab3A-GAP activity. Genes Cells 14, 41–52.
Isobe K, Raghuram V, Krishnan L, Chou CL, Yang CR, Knepper MA (2020). CRISPR-Cas9/phosphoproteomics identifies multiple non-canonical targets of myosin light chain kinase. Am J Physiol Renal Physiol 318, F600–F616.
Iwasa JH, Mullins RD (2007). Spatial and temporal relationships between actin-filament nucleation, capping, and disassembly. Curr Biol 17, 395–406.
Jean L, Majumdar D, Shi M, Hinkle LE, Diggins NL, Ao M, Broussard JA, Evans JC, Choma DP, Webb DJ (2013). Activation of Rac by Asef2 promotes myosin II-dependent contractility to inhibit cell migration on type I collagen. J Cell Sci 126, 5585–5597.
Jha A, van Zanten TS, Philippe JM, Mayor S, Lecuit T (2018). Quantitative control of GPCR organization and signaling by endocytosis in epithelial morphogenesis. Curr Biol 28, 1570–1584.e6.
Jones DH, Morris JB, Morgan CP, Kondo H, Irvine RF, Cockcroft S (2000). Type I phosphatidylinositol 4-phosphate 5-kinase directly interacts with ADP-ribosylation factor 1 and is responsible for phosphatidylinositol 4,5-bisphosphate synthesis in the golgi compartment. J Biol Chem 275, 13962–13966.
Jordens I, Fernandez-Borja M, Marsman M, Dusseljee S, Janssen L, Calafat J, Janssen H, Wubbolts R, Neefjes J (2001). The Rab7 effector protein RILP controls lysosomal transport by inducing the recruitment of dynein-dynactin motors. Curr Biol 11, 1680–1685.
Kato T, Watanabe N, Morishima Y, Fujita A, Ishizaki T, Narumiya S (2001). Localization of a mammalian homolog of diaphanous, mDia1, to the mitotic spindle in HeLa cells. J Cell Sci 114, 775–784.
Kerridge S, Munjal A, Philippe JM, Jha A, de las Bayonas AG, Saurin AJ, Lecuit T (2016). Modular activation of Rho1 by GPCR signalling imparts polarized myosin II activation during morphogenesis. Nat Cell Biol 18, 261–270.
Kimura K, Fukata Y, Matsuoka Y, Bennett V, Matsuura Y, Okawa K, Iwamatsu A, Kaibuchi K (1996). Regulation of myosin phosphatase by Rho and Rho-associated kinase (Rho-kinase). Science 273, 245–248.
Kirchner J, Gross S, Bennett D, Alphey L (2007). Essential, overlapping and redundant roles of the Drosophila protein phosphatase 1 alpha and 1 beta genes. Genetics 176, 273–281.
Kjos I, Vestre K, Guadagno NA, Borg Distefano M, Progida C (2018). Rab and Arf proteins at the crossroad between membrane transport and cytoskeleton dynamics. Biochim Biophys Acta Mol Cell Res 1865, 1397–1409.
Kuczmarski ER, Spudich JA (1980). Regulation of myosin self-assembly: phosphorylation of Dictyostelium heavy chain inhibits formation of thick filaments. Proc Natl Acad Sci USA 77, 7292–7296.
Laflamme C, Assaker G, Ramel D, Dorn JF, She D, Maddox PS, Emery G (2012). Evi5 promotes collective cell migration through its Rab-GAP activity. J Cell Biol 198, 57–67.
Lanzetti L, Palamidessi A, Areces L, Scita G, Di Fiore PP (2004). Rab5 is a signalling GTPase involved in actin remodelling by receptor tyrosine kinases. Nature 429, 309–314.
Lanzetti L, Rybin V, Malabarba MG, Christoforidis S, Scita G, Zerial M, Di Fiore PP (2000). The Eps8 protein coordinates EGF receptor signalling through Rac and trafficking through Rab5. Nature 408, 374–377.
Le K, Li CC, Ye G, Moss J, Vaughan M (2013). Arf guanine nucleotide-exchange factors BIG1 and BIG2 regulate nonmuscle myosin IIA activity by anchoring myosin phosphatase complex. Proc Natl Acad Sci USA 110, E3162–E3170.
LeBlanc MG, Lehmann R (2017). Domain-specific control of germ cell polarity and migration by multifunction Tre1 GPCR. J Cell Biol 216, 2945–2958.
Lee PL, Ohlson MB, Pfeffer SR (2015). Rab6 regulation of the kinesin family KIF1C motor domain contributes to Golgi tethering. eLife 4, e06029.
Leptin M (2005). Gastrulation movements: the logic and the nuts and bolts. Dev Cell 8, 305–320.
Leptin M, Grunewald B (1990). Cell shape changes during gastrulation in Drosophila. Development 110, 73–84.
Lindsay AJ, Jollivet F, Horgan CP, Khan AR, Raposo G, McCaffrey MW, Goud B (2013). Identification and characterization of multiple novel Rab-myosin Va interactions. Mol Biol Cell 24, 3420–3434.

Manning AJ, Peters KA, Peifer M, Rogers SL (2013). Regulation of epithelial morphogenesis by the G protein-coupled receptor mist and its ligand fog. Sci Signal 6, ra98.
Manning AJ, Rogers SL (2014). The Fog signaling pathway: insights into signaling in morphogenesis. Dev Biol 394, 6–14.
Martin AC, Goldstein B (2014). Apical constriction: themes and variations on a cellular mechanism driving morphogenesis. Development 141, 1987–1998.
Matsumura F, Hartshorne DJ (2008). Myosin phosphatase target subunit: many roles in cell function. Biochem Biophys Res Commun 369, 149–156.
McKenney RJ, Huynh W, Tanenbaum ME, Bhabha G, Vale RD (2014). Activation of cytoplasmic dynein motility by dynactin-cargo adapter complexes. Science 345, 337–341.
Miserey-Lenkei S, Chalancon G, Bardin S, Formstecher E, Goud B, Echard A (2010). Rab and actomyosin-dependent fission of transport vesicles at the Golgi complex. Nat Cell Biol 12, 645–654.
Morize P, Christiansen AE, Costa M, Parks S, Wieschaus E (1998). Hyperactivation of the folded gastrulation pathway induces specific cell shape changes. Development 125, 589–597.
Mukhopadhyay A, Nieves E, Che FY, Wang J, Jin L, Murray JW, Gordon K, Angeletti RH, Wolkoff AW (2011). Proteomic analysis of endocytic vesicles: Rab1a regulates motility of early endocytic vesicles. J Cell Sci 124, 765–775.
Mukhopadhyay A, Quiroz JA, Wolkoff AW (2014). Rab1a regulates sorting of early endocytic vesicles. Am J Physiol Gastrointest Liver Physiol 306, G412–G424.
Myers KR, Casanova JE (2008). Regulation of actin cytoskeleton dynamics by Arf-family GTPases. Trends Cell Biol 18, 184–192.
Neisch AL, Formstecher E, Fehon RG (2013). Conundrum, an ARHGAP18 orthologue, regulates RhoA and proliferation through interactions with moesin. Mol Biol Cell 24, 1420–1433.
Newell-Litwa KA, Horwitz R, Lamers ML (2015). Non-muscle myosin II in disease: mechanisms and therapeutic opportunities. Dis Model Mech 8, 1495–1515.
Nicolaï M, Lasbleiz C, Dura JM (2003). Gain-of-function screen identifies a role of the Src64 oncogene in Drosophila mushroom body development. J Neurobiol 57, 291–302.
Oishi A, Makita N, Sato J, Iiri T (2012). Regulation of RhoA signaling by the cAMP-dependent phosphorylation of RhoGDIα. J Biol Chem 287, 38705–38715.
Ojelade SA, Acevedo SF, Kalahasti G, Rodan AR, Rothenfluh A (2015). RhoGAP18B isoforms act on distinct Rho-family GTPases and regulate behavioral responses to alcohol via cofilin. PLoS One 10, e0137465.
Palamidessi A, Frittoli E, Ducano N, Offenhauser N, Sigismund S, Kajiho H, Parazzoli D, Oldani A, Gobbi M, Serini G, *et al.* (2013). The GTPase-activating protein RN-tre controls focal adhesion turnover and cell migration. Curr Biol 23, 2355–2364.
Parks S, Wieschaus E (1991). The Drosophila gastrulation gene concertina encodes a G alpha-like protein. Cell 64, 447–458.
Pearson K (1900). Mathematical contributions to the theory of evolution. VII. On the correlation of characters not quantitatively measurable. Philos Trans R Soc A Math Phys Eng Sci 195, 1–47.
Peters KA, Detmar E, Sepulveda L, Del Valle C, Valsquier R, Ritz A, Rogers SL, Applewhite DA (2018). A cell-based assay to investigate non-muscle myosin II contractility via the folded-gastrulation signaling pathway in Drosophila S2R+ cells. J Vis Exp 2018, 58325.
Peters KA, Rogers SL (2013). Drosophila Ric-8 interacts with the Gα12/13 subunit, Concertina, during activation of the Folded gastrulation pathway. Mol Biol Cell 24, 3460–3471.
Ponton F, Chapuis MP, Pernice M, Sword GA, Simpson SJ (2011). Evaluation of potential reference genes for reverse transcription-qPCR studies of physiological responses in Drosophila melanogaster. J Insect Physiol 57, 840–850.
Rahmsdorf HJ, Malchow D, Gerisch G (1978). Cyclic AMP-induced phosphorylation in Dictyostelium of a polypeptide comigrating with myosin heavy chains. FEBS Lett 88, 322–326.
Rayment I, Holden HM, Whittaker M, Yohn CB, Lorenz M, Holmes KC, Milligan RA (1993a). Structure of the actin-myosin complex and its implications for muscle contraction. Science 261, 58–65.
Rayment I, Rypniewski WR, Schmidt-Bäse K, Smith R, Tomchick DR, Benning MM, Winkelmann DA, Wesenberg G, Holden HM (1993b). Three-dimensional structure of myosin subfragment-1: a molecular motor. Science 261, 50–58.
Reid T, Furuyashiki T, Ishizaki T, Watanabe G, Watanabe N, Fujisawa K, Morii N, Madaule P, Narumiya S (1996). Rhotekin, a new putative target for Rho bearing homology to a serine/threonine kinase, PKN, and rhophilin in the rho-binding domain. J Biol Chem 271, 13556–13560.
Ricketson D, Johnston CA, Prehoda KE (2010). Multiple tail domain interactions stabilize nonmuscle myosin II bipolar filaments. Proc Natl Acad Sci USA 107, 20964–20969.
Rodriguez OC, Cheney RE (2002). Human myosin-Vc is a novel class V myosin expressed in epithelial cells. J Cell Sci 115, 991–1004.
Rogers SL, Rogers GC (2008). Culture of Drosophila S2 cells and their use for RNAi-mediated loss-of-function studies and immunofluorescence microscopy. Nat Protoc 3, 606–611.
Rogers SL, Wiedemann U, Häcker U, Turck C, Vale RD (2004). Drosophila RhoGEF2 associates with microtubule plus ends in an EB1-dependent manner. Curr Biol 14, 1827–1833.
Rogers SL, Wiedemann U, Stuurman N, Vale RD (2003). Molecular requirements for actin-based lamella formation in Drosophila S2 cells. J Cell Biol 162, 1079–1088.
Roland JT, Bryant DM, Datta A, Itzen A, Mostov KE, Goldenring JR (2011). Rab GTPase-Myo5B complexes control membrane recycling and epithelial polarization. Proc Natl Acad Sci USA 108, 2789–2794.
Roland JT, Kenworthy AK, Peranen J, Caplan S, Goldenring JR (2007). Myosin Vb interacts with Rab8a on a tubular network containing EHD1 and EHD3. Mol Biol Cell 18, 2828–2837.
Rousso T, Shewan AM, Mostov KE, Schejter ED, Shilo BZ (2013). Apical targeting of the formin Diaphanous in Drosophila tubular epithelia. eLife 2, e00666.
Schlager MA, Kapitein LC, Grigoriev I, Burzynski GM, Wulf PS, Keijzer N, de Graaff E, Fukuda M, Shepherd IT, Akhmanova A, *et al.* (2010). Pericentrosomal targeting of Rab6 secretory vesicles by Bicaudal-D-related protein 1 (BICDR-1) regulates neuritogenesis. EMBO J 29, 1637–1651.
Scholey JM, Taylor KA, Kendrick-Jones J (1980). Regulation of non-muscle myosin assembly by calmodulin-dependent light chain kinase. Nature 287, 233–235.
Sellers JR, Pato MD, Adelstein RS (1981). Reversible phosphorylation of smooth muscle myosin, heavy meromyosin, and platelet myosin. J Biol Chem 256, 13137–13142.
Silver JT, Wirtz-Peitz F, Simões S, Pellikka M, Yan D, Binari R, Nishimura T, Li Y, Harris TJC, Perrimon N, *et al.* (2019). Apical polarity proteins recruit the RhoGEF cysts to promote junctional myosin assembly. J Cell Biol 218, 3397–3414.
Somlyo AP, Somlyo AV (2000). Signal transduction by G-proteins, rho-kinase and protein phosphatase to smooth muscle and non-muscle myosin II. J Physiol 522(Pt 2), 177–185.
Spinner MA, Walla DA, Herman TG (2018). Syd-1 has RhoGAP activity that is required for presynaptic clustering of Bruchpilot/ELKS but not neurexin-1. Genetics 208, 705–716.
Su Z, Kiehart DP (2001). Protein kinase C phosphorylates nonmuscle myosin-II heavy chain from Drosophila but regulation of myosin function by this enzyme is not required for viability in flies. Biochemistry 40, 3606–3614.
Tahirovic S, Hellal F, Neukirchen D, Hindges R, Garvalov BK, Flynn KC, Stradal TE, Chrostek-Grashoff A, Brakebusch C, Bradke F (2010). Rac1 regulates neuronal polarization through the WAVE complex. J Neurosci 30, 6930–6943.
Tan C, Stronach B, Perrimon N (2003). Roles of myosin phosphatase during Drosophila development. Development 130, 671–681.
Tanna CE, Goss LB, Ludwig CG, Chen PW (2019). Arf GAPs as regulators of the actin cytoskeleton—an update. Int J Mol Sci 20, 442.
Trotter JA (1982). Living macrophages phosphorylate the 20,000 dalton light chains and heavy chains of myosin. Biochem Biophys Res Commun 106, 1071–1077.
Trotter JA, Nixon CS, Johnson MA (1985). The heavy chain of macrophage myosin is phosphorylated at the tip of the tail. J Biol Chem 260, 14374–14378.
Trybus KM (1989). Filamentous smooth muscle myosin is regulated by phosphorylation. J Cell Biol 109, 2887–2894.
Turbedsky K, Pollard TD, Yeager M (2005). Assembly of Acanthamoeba myosin-II minifilaments. Model of anti-parallel dimers based on EM and X-ray diffraction of 2D and 3D crystals. J Mol Biol 345, 363–373.
Uehara R, Goshima G, Mabuchi I, Vale RD, Spudich JA, Griffis ER (2010). Determinants of myosin II cortical localization during cytokinesis. Curr Biol 20, 1080–1085.
Ueno H, Huang X, Tanaka Y, Hirokawa N (2011). KIF16B/Rab14 molecular motor complex is critical for early embryonic development by transporting FGF receptor. Dev Cell 20, 60–71.

Umemoto S, Bengur AR, Sellers JR (1989). Effect of multiple phosphorylations of smooth muscle and cytoplasmic myosins on movement in an in vitro motility assay. J Biol Chem 264, 1431–1436.
Vasquez CG, Tworoger M, Martin AC (2014). Dynamic myosin phosphorylation regulates contractile pulses and tissue integrity during epithelial morphogenesis. J Cell Biol 206, 435–450.
Verdier V, Guang-Chao-Chen, Settleman J (2006). Rho-kinase regulates tissue morphogenesis via non-muscle myosin and LIM-kinase during Drosophila development. BMC Dev Biol 6, 38.
Vestre K, Kjos I, Guadagno NA, Borg Distefano M, Kohler F, Fenaroli F, Bakke O, Progida C (2019). Rab6 regulates cell migration and invasion by recruiting Cdc42 and modulating its activity. Cell Mol Life Sci 76, 2593–2614.
Vicente-Manzanares M, Horwitz AR (2010). Myosin light chain mono- and diphosphorylation differentially regulate adhesion and polarity in migrating cells. Biochem Biophys Res Commun 402, 537–542.
Vicente-Manzanares M, Koach MA, Whitmore L, Lamers ML, Horwitz AF (2008). Segregation and activation of myosin IIB creates a rear in migrating cells. J Cell Biol 183, 543–554.
Vicente-Manzanares M, Ma X, Adelstein RS, Horwitz AR (2009). Non-muscle myosin II takes centre stage in cell adhesion and migration. Nat Rev Mol Cell Biol 10, 778–790.
Waterman-Storer CM, Desai A, Bulinski JC, Salmon ED (1998). Fluorescent speckle microscopy, a method to visualize the dynamics of protein assemblies in living cells. Curr Biol 8, 1227–1230.
West-Foyle H, Kothari P, Osborne J, Robinson DN (2018). 14-3-3 proteins tune non-muscle myosin II assembly. J Biol Chem 293, 6751–6761.
Wilkinson S, Paterson HF, Marshall CJ (2005). Cdc42-MRCK and Rho-ROCK signalling cooperate in myosin phosphorylation and cell invasion. Nat Cell Biol 7, 255–261.
Winkelmann DA, Almeda S, Vibert P, Cohen C (1984). A new myosin fragment: visualization of the regulatory domain. Nature 307, 758–760.
Woroniuk A, Porter A, White G, Newman DT, Diamantopoulou Z, Waring T, Rooney C, Strathdee D, Marston DJ, Hahn KM, *et al*. (2018). STEF/TIAM2-mediated Rac1 activity at the nuclear envelope regulates the perinuclear actin cap. Nat Commun 9, 2124.
Xie S, Mason FM, Martin AC (2016). Loss of Gα12/13 exacerbates apical area dependence of actomyosin contractility. Mol Biol Cell 27, 3526–3536.
Yamashiro S, Totsukawa G, Yamakita Y, Sasaki Y, Madaule P, Ishizaki T, Narumiya S, Matsumura F (2003). Citron kinase, a Rho-dependent kinase, induces di-phosphorylation of regulatory light chain of myosin II. Mol Biol Cell 14, 1745–1756.
Yin HL, Janmey PA (2003). Phosphoinositide regulation of the actin cytoskeleton. Annu Rev Physiol 65, 761–789.
Yuen SL, Ogut O, Brozovich FV (2009). Nonmuscle myosin is regulated during smooth muscle contraction. Am J Physiol Heart Circ Physiol 297, H191–H199.